Coaxial Bioprinter Design & Validation

A vascular solution to a perfusable future

AE5822: Masters Thesis

Matas Venčkauskas

Delft University of Technology

TU Delft

Coaxial Bioprinter Design & Validation

A vascular solution to a perfusable future

by

Matas Venčkauskas

Supervisor:	K. Masania
Supporting Supervisor:	M. Ablonczy
Supporting Supervisor:	S. Bhusari
Project Duration:	February, 2025 - November, 2025
Faculty:	Faculty of Aerospace Engineering, Delft

Cover: Ultishmoomaker modular nozzles by Matas Venčkauskas
Style: TU Delft Report Style, with modifications by Daan Zwaneveld

TU Delft

Acknowledgement

I would like to express my sincere gratitude to my supervisors, Dr. K. Masania, M. Ablonczy, and S. Bhusari, for their invaluable guidance, patience, and technical insight throughout the development of this project. Their expertise and encouragement were essential in shaping both the direction and quality of this work.

I would also like to thank the technicians at the Faculty of Aerospace Engineering for their practical assistance, resourcefulness, and support in overcoming many of the experimental and fabrication challenges encountered during this research.

Special thanks go to my friends David, Radha, and Silvan for their constant motivation, perspective, and for making the long hours in the lab more enjoyable. I am equally grateful to my physics friends Paulius and Elena, whose curiosity, discussions, and humor helped me stay grounded and inspired.

Further, I want to thank my spiritual mentors Jonatan Leandoer, Anthony Hawk and Adam Savage. The unrelenting, creative and curious ways that they have led me through my life, are cemented in this work and proliferate in the ways that I see, design and create.

Finally, I wish to extend my heartfelt appreciation to my parents and family, whose unwavering support, patience, and belief in my abilities have carried me through every challenge. This work would not have been possible without their encouragement and understanding.

Abstract

Vasculatures are key components to life, enabling transport of critical life-sustaining fluids, like blood in humans, or water in trees. To make artificial structures that exhibit characteristics of life, it is important to mimic nature and enable vascularization for human-made materials. The technology to print vascular materials exists, but there are major challenges regarding how to integrate these materials, and their industrial scalability. This thesis investigates coaxial bioprinting as a scalable option and details the design, development, and validation of a coaxial extrusion-based bioprinter engineered for the fabrication of perfusable calcium alginate vascular structures. The outcome of the design process was a new coaxial nozzle capable of printing controlled and consistent vascularized alginate structures directly onto a print bed. This is a key step enabling scalable vasculature manufacturing as the use of printing baths and gels is completely avoided. The printers capabilities were then validated and found to meet the initial design specifications. Further, the accuracy of printing planar features was quantified followed by demonstrations of fully perfusable 3D prints. Results show that the vasculature's inner channel size can be controllably tuned by varying the nozzle size combinations, enabled by the new nozzle design. In addition, the geometry of the extrusion can be controllably tuned while printing by varying the extrusion factor. Experiments showed that the printer can handle printing sharp angles with an error of up to 10 degrees, which enables complex vascularized shapes. Additionally, curves were shown to be printed accurately at radius of half of that of the diameter of the vasculature and larger. Bridging testing resulted in a optimal setting of extrusion factor to bridge 25mm gaps at a height of 5mm. The final design fulfils all predefined functional and performance requirements, confirming the feasibility of modular coaxial bioprinting for vascular fabrication. The resulting platform provides a truly cost-effective and scalable foundation for manufacturing man-made vascularized structures.

Contents

List of Figures

List of Tables

Nomenclature

Abbreviations

Abbreviation	Definition
SLA	Stereolithography
LIFT	Laser induced forward transfer
USM	Ultishmoomaker
FDM	Fused deposition modelling
GelMa	Gelatin Methacrylate
EF	Extrusion factor
IN	Inner needle
ON	Outer needle
IR	Inner radius
OR	Outer radius
ID	Inner diameter
OD	Outer diameter
UM2+	Ultimaker 2+
EDTA	Ethylenediaminetetraacetic acid
COTS	Commercial off the shelf acid

1

Introduction

1.1. Problem Statement

Vasculatures exist all around us - in the tree canopies that give us shade, in the fibres of flax used to make rope, in the linen that makes up our pants and in our very own bodies as blood vessels. Vasculatures are a key mechanism of almost all lifeforms found on earth carrying fluids and nutrients across the organism. Without vasculatures much of life on earth would cease to exist in an instant. Trees require vasculatures to not only carry fluids but vasculatures also provide an optimal structure maximising specific strength and stiffness. However, the harvest of vascular materials like wood results in the death of the underlying life that had earlier formed the desired vasculatures. Thus, to make human-made materials with the benefits of living functionalities - like self-healing and biosensing - it is important to embed them with vasculatures. The potential application space for living biomaterials is increasing in civil, space and other fields of engineering, for both sustainability, but sensing features as well. However, to become useful vascular printing must be applicable in a scalable, industrial manner. Methods like SLA, in-gel and in-bath have been often used for smaller scale applications, however, are not scalable and are restricted by the size of their baths. This is a major flaw in the current systems, that would not allow for the integration in multi-material manufacturing. This flaw also prevents significant scaling, before such systems simply become too expensive, large and over complicated. Moreover, to harness the powers of vasculatures found in nature in nutrient delivery, the perfusability of vasculatures must be a controllable function when printing. Thus, the problem statement is - **how to build a vasculature printing technology that is biocompatible, scalable and allows for perfusion.**

1.2. State of The Art

There are four methods used to print artificial vascular biomaterials. These are: SLA, in-gel, in-bath and coaxial direct extrusion. SLA (stereolithography) is a method that uses light to selectively crosslink areas of light sensitive ink in a bath. SLA can achieve sub 100 micron resolutions, however, the need for a bath, light sensitive bioinks, hampers the scalability, while the process is prone to entrapment of ink. Next, the in-gel printing method uses direct extrusion of a bioink that crosslinks in a gel bath, that offers support. Researchers have demonstrated the use of in-gel printing to print a vascularised heart[1] in sacrificial gelatine bath. Here, similar scalability drawbacks occur as with all bath methods, moreover perfusability is equally challenging in SLA and in-gel due to entrapped ink. A similar method is in-bath printing, where extrusion occurs into a wet crosslinker bath, where support is generated traditionally (with support structures). When paired with a coaxial nozzle (where a core-shell filament can be extruded) vascular structures can be printed directly. However, as with all bath-based approaches similar drawbacks are present, but perfusability is improved, since the vascularised lumen is continuous and only one perfusion interface is needed. The last method of coaxial direct extrusion is similar to the previous, it prints a core-shell filament, however without a bath - like a direct ink method. This approach, unlike its counterparts, is not constrained by a bath, meaning that vasculatures can be extruded anywhere, making it scalable. Due to the coaxial nature, perfusability is simplified with only one interface necessary. For all methods repeatable or consistent perfusion interfaces are not trivial and

require further investigation. Regarding the kinds of inks used to form vasculatures, biocompatible inks are available for all methods, but to varying extents, where ones for direct extrusion based methods have been most developed and are considered most reliable [2]. To summarize, there are quite a few existing ways how to produce biocompatible vascular materials, although the technology to produce them at scale is not yet mature.

1.3. Research Gap

As seen in the previous section, there are multiple ways that vascular printing could be accomplished, however, the main issues of scalability, perfusability and biocompatibility are not completely solved. Scalability is one of the apparent largest research gaps. For example, vasculatures printed in baths or gels cannot be easily scaled or integrated in multi-material manufacturing processes. This is important if vascular bio structures are to be implemented in large components such as air plane interiors, off-planet shelters and bridges back here on earth. Additionally, perfusability is important to address. The gap is that existing technologies are challenging to perfuse with liquids and achieve the kind of circulation in natural vasculatures. This is important since a vasculature is only truly useful if the lumen can be utilised to carry nutrients, organism cultures or other relevant fluids. Thus, the ability to perfuse in a repeatable and consistent manner is highly important. Laslty, the biocompatibility of inks and the printing process is the final research gap. Many inks can be used to make vascular structures, but one important constraint alongside scalability and perfusability is that the used ink technology must be biocompatible. There is also an important gap in the understanding of the effect of the printing process on the properties and the biocompatibility of the used bioinks. This includes the understanding that is necessary to control the vasculature formation. In summary, the research gaps that this thesis seeks to address are: (1) scalable and integratable manufacturing technology, (2) consistent perfusability, (3) understanding the effects of the printing process on the bioinks.

1.4. Research Objective

Building on the identified research gaps in scalability, perfusability, and biocompatibility of vascular printing, this thesis focuses on addressing the fundamental limitation of scalability by developing a coaxial printing approach that is not confined to a support bath.

The main research objective of this thesis is to design a 3D coaxial bioprinter capable of using biocompatible inks to fabricate perfusable vascular structures.

This research objective can be broken down into 3 main elements:

1. To develop a coaxial nozzle & printer, that facilitates direct ink writing without a bath or gel.
2. To develop new printing techniques that enable printing consistent and perfusable vasculatures.
3. To validate the performance and reliability of the printer system.

The development of the coaxial nozzle provides the hardware foundation for the printing process and directly addresses the scalability challenge. This is followed by the development of the printing process itself, with the aim of understanding and controlling the parameters that govern the resulting vascular prints. Finally, the validation of the printer system confirms its performance and functionality, addressing the overarching research gaps.

1.5. Research Questions

To achieve the previously mentioned research objective, research questions allow to formulate a more concise approach. The main research questions guiding this thesis are:

1. How do extrusion parameters and coaxial nozzle geometries influence the formation, stability, and inner diameter of perfusable vascular structures printed with biocompatible inks?
2. How accurately can the bioprinter reproduce planar geometric features—such as sharp angles, radii, and complex contours—using coaxial vascular printing, and what errors arise during their

formation?

3. How can the printer achieve fully perfusable 3D vascular prints, including bridged layers and demonstrator structures like cylinders and lattices, and what factors influence this process?

The first question investigates the properties of printer vasculatures and the effects on their geometries and formation behaviour. This is the first building block to 3D printing. Next, the second question explores what are the limits of planar printing and what are the effects of of the resulting prints. Lastly, this is then built upon through the last research question which explores the possibilities in multilayer 3D printing and provides insight to novel bridging features enabled by coaxial printing.

1.6. Thesis Structure

This section presents the outline of the thesis. With the stated motivations in mind, first a literature study in chapter 2 was conducted to better understand the existing approaches and their application. Next, chapter 3 seeks to present the design process of the printer that was used to research the vasculature printing process. This is then followed by chapter 4 where the coaxial printing process is investigated further. Here, the experiments validating the printer are presented and their results are discussed. Lastly, chapter 5 provides a summary of the relevant conclusions of the thesis, while also giving recommendations and insight on the future of this technology and research.

2

Coaxial Bioprinting Literature Study

Coaxial bioprinting is a niche yet intriguing field for the future of research, bio-medical applications and even space travel. This project is concerned with the design of a bioprinter capable of printing vasculatures with various inks, for applications in the field of engineered living materials. To set a solid foundation for the thesis, a literature study was conducted, investigating various aspects of bioprinters and their operations. Here, section 2.1 present the cutting edge of bioprinting, with a focus on vasculature printing.

2.1. Bioprinting

Bioprinting is a type of additive manufacturing that combines conventional 3D printing techniques with the use of bioinks, cells, nutrients to manufacture functional structures often used for tissue engineering and possibly for biosensing and other applications in the future [3][4][5][6]. The potential benefits of bioprinting are abundant and impactful for the future of biomedical applications and space exploration. 3D bioprinting is crucial in the development and construction of artificial tissues and organs. At the present, organs such as: a heart seen in Figure 2.1, liver, lung, kidney, have already been constructed using state of the art bioprinting methods [7]. In Figure 2.1 a customised extrusion-based method FRESH [1] was used.

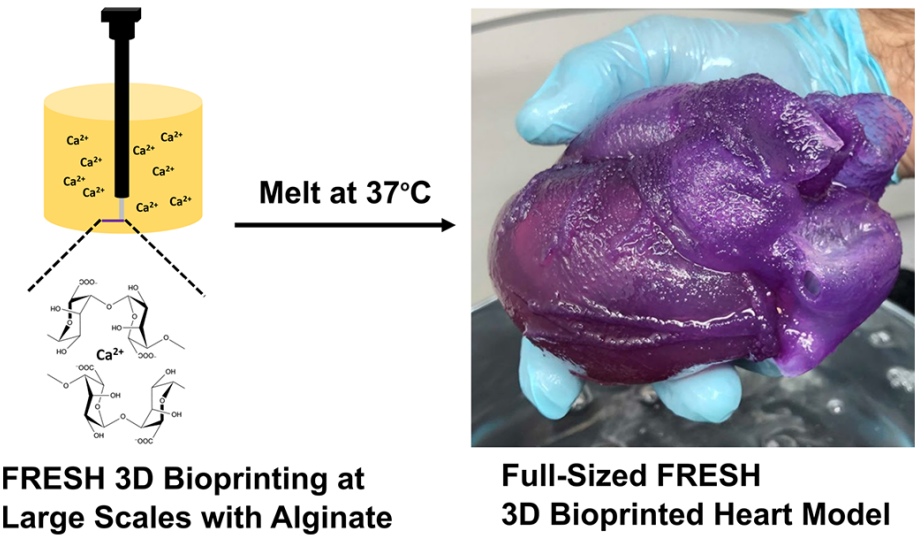

Figure 2.1: Heart printed from alginate using FRESH method [1]

Bioprinting Methods

To better understand the implications of the approaches used to bioprint it is important to examine the state of the art. The state of the art methods are as follows:

- Inkjet
- Stereolithography (SLA)
- Laser induced forward transfer (LIFT)
- Extrusion

Illustrations for each method can be seen in Figure 2.2 The inkjet method is the oldest among the group mentioned. Essentially during the inkjet process small droplets are deposited on a surface either using piezo actuation or heating. Advantages are that this method is low cost, prints at a high speed and no contact with the substrate means that contamination can be prevented. However, this method requires bioinks of low viscosity, limited to <15mPa. Additionally, the deposition occurs in the pico-litre size range subject to very high evaporation, detrimental to cell survival. Next, the SLA method utilises a laser beam to cure the ink selectively layer by layer. This method offers a micrometer resolution allowing for fine porosity adjustment. However, the photosensitive constraint for the bioink narrows the possible ink selection drastically. This means the selection for cell cultures is reduced due to ink incompatibilities. To make matters worse, the UV exposure during SLA is also detrimental to cells. Thus, the viability of SLA is reduced drastically. This leads to LIFT printing. LIFT produces droplets by shining a laser onto a donor layer beneath which the bioink is suspended. This light creates a vapor bubble which causes the ink to be deposited. The advantages are that his is a non-contact method and unlike inkjet it is not prone to clogging due to living material settling out. More, the viscosity range is higher than inkjet (1-300mPa) and cell density can be higher as well. However, the preparation of the bi-layer ribbon with donor and bioink is very time intensive, the generation of droplets is erratic and this method is high cost. Last but not least, the extrusion-based methods. Extrusion-based methods are used the most abundant and are very similar to fused deposition modelling (FDM). This method can print very cell dense and viscous inks, through either pneumatic, piston or screw driven extrusion. This method is also cheap to set up, as conventional FDM printers can be quickly converted. Additionally, heterogeneous prints are possible, this is important when printing things like organs where the placement of different cell cultures in space is crucial. Importantly, the extrusion-based approaches has been proven by printing things like the heart in Figure 2.1 and have a large subset of customisations for specific applications. [8]

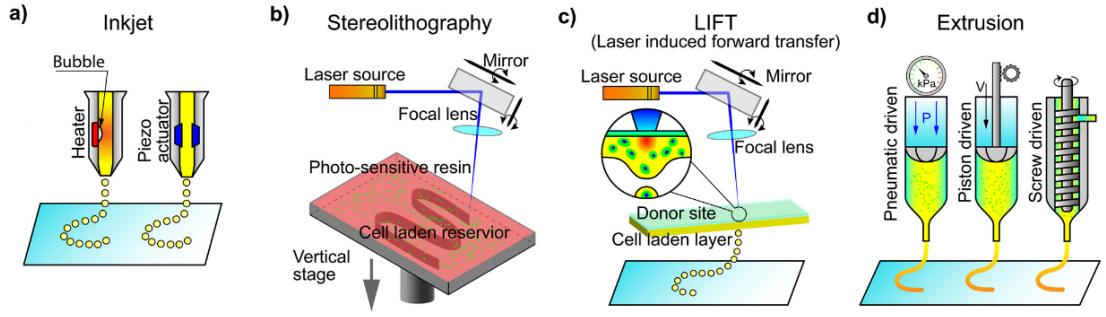

Figure 2.2: Bioprinting methods: inkjet, SLA, LIFT and extrusion [8]

Considering the various approaches, an extrusion-based approach is most sensible considering the ease of implementation, affordability, ink selection versatility, existing literature and customisations. However, extrusion-based approaches are categorised using the extrusion method and the working mechanisms. The extrusion methods are depicted in Figure 2.2. Pneumatic-based extrusion is popular, it operates by providing a compressed gas at a specified pressure to a piston/syringe to extrude the bio ink. However, it encounters delays in extrusion-based on the rheological properties of the bio inks, which is not very convenient. Screw-based extrusion uses a turning screw to extrude material. The benefits of this method is that it is well suited for high viscosity inks, however it is prone to causing damage to the cells laden in the ink (however there can be modifications applied to prevent this) [9].

Lastly, the mechanical piston is a syringe that is driven by a motor and dispenses the bio ink mechanically. Considering the aforementioned, the piston driven extrusion method is arguably the most reliable, simple and easy to set up.

Bioprinting Working Mechanisms

This leads to the next consideration - the working mechanisms. This can be described as the crosslinking mechanism that defines the process:

- direct extrusion
- extrusion into a coagulation bath
- extrusion into a support bath
- extrusion onto a framework
- coaxial extrusion

Direct extrusion is uses shear thinning, where the fluid in motion is less viscous and gels up when stationary to hold its shape. Extrusion into a coagulation bath is done by extruding an ink into a bath that crosslinks on the ink on contact. Here the shear thinning requirement is omitted, but this process is prone to severe clogs. Printing into a support bath removes the need for a support structure and allows for omni directional deposition of ink, but requires a full volume bath. This is the same method that heart using the FRESH method in Figure 2.1 was made with, utilizing a GelMa slurry bath that could then be melted away. Extruding onto a framework is similar to the support bath in the sense that support is provided, but the supporting structure is ”the framework” a rigid shape such as a mandrel. This approach is interesting, but inflexible comparatively. Last, coaxial printing allows for the printing of core shell structures. This approach combines the FDM approach of direct ink printing with the coagulation approach by extruding two crosslinking inks through two concentric needles as in Figure 2.3.

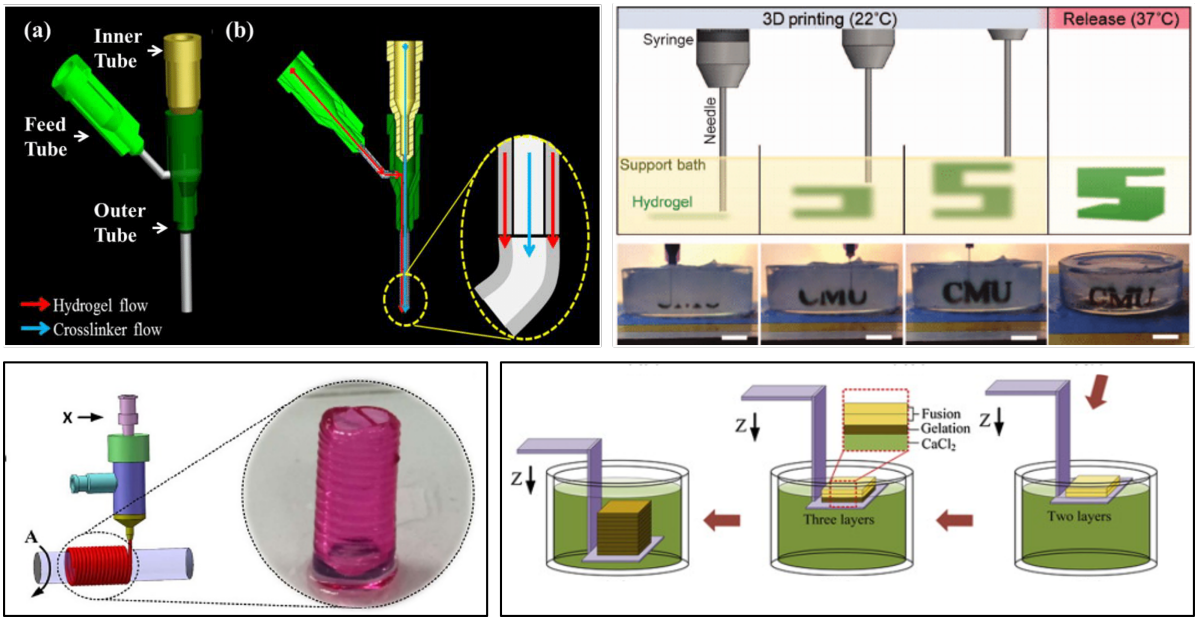

Figure 2.3: Extrusion working mechanisms: coaxial (top left) by Yahui Zhang, onto framework (bottom left) [6], into support bath (top right) [10], into coagulant bath (bottom right) [2]

Here, the two inks crosslink forming a shell filament that can be deposited, and in the case of sodium alginate and calcium chloride inks later perfused. Notably, the coaxial method can also use shear thinning inks as well, or UV crosslinking ones to create a core shell [6]. Thus, depending on the composition of the bio-ink it becomes possible to inoculate the inks with nutrients or organisms, and crosslink the core-shell structure either during the printing process or even after. Comparing coaxial printing, to the other options mentioned, coaxial printing is more versatile than:

- direct extrusion, because if needed it can easily do it as well
- in coagulation bath extrusion, because the same effect could be achieved by reversing the ink injection (e.g. alginate inside, calcium chloride outside.
- in support bath extrusion, because there is no cumbersome bath needed to create vascular or enclosed features.
- onto framework extrusion, because coaxial extrusion is not limited by a mandrel or any other framework.

Additionally, coaxial extrusion could be directly applied in all cases if necessary to combine the strengths of each working mechanism. However, to take advantage of the vascular nature of coaxial printing a particular selection of inks should be investigated.

Bioinks for Coaxial Printing

Many ink formulations have been used for coaxial printing and provide different benefits through different levels of porosity, bio-compatibility, storability etc. One of the most significant bio inks is sodium alginate - a natural polysaccharide derived from brown seaweed, composed of mannuronic and guluronic acid units. It forms viscous solutions and hydrogels, making it useful in food processing, pharmaceuticals, and biomedical applications such as cell encapsulation and 3D bioprinting [11]. The natural crosslinker of alginate is calcium chloride - an inorganic salt that releases calcium ions in solution, which cross-link with alginate to form stable hydrogels. This reaction underlies its use in spherification, tissue engineering, and food preservation [12]. Popping boba balls (Figure 2.4) are made using these very bio-inks! The resulting calcium alginate hydrogel is elastic, biocompatible and quick forming which is why it has extensively been used in the bioprinting domain. The optimal formulation has been previously found to be 4% W/V (weight per volume, for both alginate and calcium chloride) for best vasculature formation, stiffness and sufficient cell proliferation properties [2]. However, alginate is slow to degrade which is not desirable in printed organs and such and is said to have low cell proliferation in general.

Figure 2.4: A refreshing cup of Boba tea with popping boba balls made with alginate (left), Kelp (middle) by Bjorn Christian Torrissen, Genipa Americana (right) by Joao Medeiros

Additionally, an extensive list of alternative bio-inks can be seen in Table A.1. Here, an alternative is chitosan - a natural, semi-crystalline, linear polymer. The gelation pairing for this ink would be dialdehyde crosslinkers or Genipin, an extract of the naturally occurring Genipa americana. However, the use of chitosan is not extensive. In a direct vascular setting compared against alginate it became evident that chitosan vasculatures suffer from inferior mechanical properties and therefore rupture. In light of both the inferiorities of alginate and chitosan, some researchers have made composite variations of both with carbon nanotubes [13] to strengthen alginate or added GelMA (Gelatin Methacrylate) to alginate [14] to support better proliferation. All in all, alginate is superior since it is cheap, mechanically strong and elastic, crosslinks rapidly and allows for the tuning of its gelation. [6]

Limitations and Challenges

Coaxial printing has limitations in terms of clogging. As mentioned in [6] the biggest limitation is related to printing in baths where clogging occurs very quickly, failing the attempted bioprint. Additionally, due to the nature of the small orifices and tight gaps in between the coaxial needles, even small amounts

of cross-contamination can destroy a nozzle indefinitely. This when paired with the price of a coaxial needle from a supplier like Sigma-Aldrich (around 200 EUR per needle) can easily become a thousand euros worth of mistakes during a printing session. This is not the case in SLA and other types of bioprinting and is a direct result of the crosslinking approach.

Moreover, the lumen of the vasculature can close shut if too sharp of an angle is made during printing. This can ruin the perfusability of the vasculature print. Alongside this, the difficulties of creating bifurcated vascular constructs (Y and T junctions) make replicating anatomical vascular structures difficult. Apparently, this can be done manually but not consistently or with scalability in mind. In addition, coaxial printing may encounter issues commonly shared with other conventional extrusion-based methods. Extrusion pressure and shear can negatively affect cell viability, particularly in the inner core where flow is constrained. This combined with a particularly viscous ink prone to low proliferation and the screw method of extrusion could compound to ruin the results of such a bioprint. [6]

3

Bioprinter Design

The journey from command to vasculature is a story of design, failure, and persistence. This chapter recounts the evolution of the bioprinter, capturing both the creative process and the engineering challenges faced throughout development. It begins with section 3.1, which defines the design requirements, followed by section 3.2, outlining the initial printer configuration. The following section, section 3.3, details the hardware and software development of the system, culminating in section 3.4, which presents the specifications of the final design.

3.1. Design Requirements

To successfully design and develop the bioprinter, it is essential to begin with a clearly defined set of system requirements. Establishing these requirements at the outset provides a structured framework that guides design decisions, constrains the project scope, and ensures that development remains aligned with the intended function of the system. Furthermore, explicit requirements are crucial for **verification and validation**, allowing each design iteration to be tested and confirmed against measurable criteria.

The **SMART** methodology was adopted to formulate these requirements, ensuring that each one is both actionable and verifiable. This framework promotes clarity and accountability, making it possible to track progress through objective performance indicators. The acronym SMART stands for:

- **Specific:** Each requirement targets a clearly defined aspect of system performance or functionality.
- **Measurable:** The outcome can be quantified or objectively evaluated through testing or inspection.
- **Assignable:** Responsibility for meeting the requirement can be traced to a subsystem, component, or development stage.
- **Realistic:** The target is achievable within the available resources, time, and technical constraints.
- **Time-related:** The requirement aligns with the project timeline and design milestones.

This structured approach helps prevent scope drift. The resulting set of requirements, presented in Table 3.1, was chosen to capture the essential capabilities and engineering constraints needed to realize a functional coaxial bioprinter. These requirements reflect a balance between the research objectives of printing perfusable vasculatures and the mechanical and software constraints inherent in adapting an existing 3D printing platform.

#	REQ ID	Description	Justification	Validation Method
1	MYCO-PRNT-01	The 3D printer shall produce prints capable of perfusion of 20 ml	Vital function of a vasculature	Test
2	MYCO-CAD-01	The 3D printer software suite shall allow for slicing .stl and .3mf files	Necessary for quick development cycles	Review of Design
3	MYCO-PRNT-02	The 3D printer shall be able to print vasculatures of 3 different ID	Requested by users	Test
4	MYCO-SAFE	The 3D printer shall have measures to prevent user error damage to the printer	Prevent premature failure of system	Review of Design, Inspection
5	MYCO-DESIGN-01	The 3D printer shall have a modular nozzle	Need for non interrupted printing	Review of Design, Inspection
6	MYCO-INK	The 3D printer shall support printing in alginate and calcium chloride	Available materials	Review of Design
7	MYCO-PRNT-04	The 3D printer shall print perfusable planar angles with an error after the feature, no greater than 10 deg	Proof of predictable printing quality	Test
8	MYCO-PRNT-05	The 3D printer shall print perfusable planar radii with an error after the feature, no greater than 20%	Proof of predictable printing quality	Test
9	MYCO-PRNT-06	The 3D printer shall be able to print a perfusable structures of 4cm in height	Proof of 3D capabilities	Test
10	MYCO-DESIGN-02	The modular nozzle shall not leak	Leaking introduces error in the printing process	Review of Design, Inspection
11	MYCO-DESIGN-03	The distance between the inner and outer needle walls shall be larger than 1 wall thickness of the inner needle	Ensures concentricity	Review of Design, Inspection

Table 3.1: List of base printer requirements

Each requirement in Table 3.1 was strategically selected to ensure the final system would be functional, adaptable, and verifiable:

- **MYCO-PRNT-01** establishes the fundamental performance benchmark: the printer must produce constructs capable of sustaining a perfusion of 20ml. This quantifiable target directly validates vascular functionality and provides an objective measure of successful bioprinting.
- **MYCO-CAD-01** specifies compatibility with commonly used CAD formats (.stl and .3mf), enabling efficient iteration cycles. Since design changes are frequent during experimental optimization, seamless slicing support ensures a smooth workflow and reduces downtime.
- **MYCO-PRNT-02** requires the printer to fabricate vasculatures of three distinct inner diameters. This ensures the system can accommodate a range of lumen sizes relevant for applications with differing flow, diffusion, and structural requirements.
- **MYCO-SAFE** introduces essential reliability constraints. By incorporating measures that protect against user-induced damage, the system remains robust during experimentation—particularly important in environments involving repeated handling, calibration, and parameter adjustments.
- **MYCO-DESIGN-01** guarantees compatibility with commercial off-the-shelf (COTS) needles, en-

suring that the nozzle assembly is modular, easily replaceable, and adaptable. This supports uninterrupted printing, rapid maintenance, and future integration of alternative needle geometries.

- **MYCO-INK** ensures that the system supports printing with alginate and calcium chloride, the two materials fundamental to coaxially crosslinked hydrogel formation. These bioinks were selected for their availability, safety, and compatibility with coaxial extrusion, as discussed in chapter 2.
- **MYCO-PRNT-04** provides a quantifiable measure of planar printing fidelity by requiring that angular features deviate no more than 10 after the feature. This metric evaluates nozzle control, extrusion responsiveness, and motion synchronization in two-dimensional paths.
- **MYCO-PRNT-05** extends the fidelity assessment to curved features, requiring planar radii to deviate no more than 20% from their intended geometry. This criterion evaluates the printer's ability to maintain stable extrusion and accurate motion during continuous curvature.
- **MYCO-PRNT-06** defines the required three-dimensional capability: the system must reliably produce perfusable structures at least 4cm in height. This ensures that the coaxial extrusion process remains stable and aligned throughout volumetric deposition.
- **MYCO-DESIGN-02** requires that the modular nozzle assembly must not leak, as leakage introduces extrusion inconsistencies and dimensional inaccuracies in the printed constructs.
- **MYCO-DESIGN-03** ensures proper geometric alignment by requiring the radial distance between the inner and outer needles to exceed one wall thickness of the inner needle. This promotes concentricity critical to shell formation.

Collectively, these requirements ensure that the final printer is not only capable of producing functional vascular-like structures, but also remains safe, modular, and adaptable for future research applications.

With the requirements established, the next step was to identify a suitable foundation on which to build the bioprinter. The chosen platform needed to balance accessibility, modifiability, and precision to satisfy the criteria outlined in Table 3.1. The Ultimaker 2+ was selected as the base system due to its open mechanical architecture, robust motion control, and readily available modification ecosystem. Its reliable kinematic structure, combined with the ease of firmware and hardware customization, made it an ideal starting point for developing a coaxial bioprinting platform. The following section, section 3.2, introduces this initial configuration in detail and discusses its role as the groundwork for subsequent hardware and software development.

3.2. Original Printer

To understand the development path of the bioprinter, it is first necessary to define the starting point of the system. This section presents the initial hardware and software configuration that served as the foundation for all subsequent modifications.

First, it is important to note the framework that is used to build the bioprinter. In this case it is the Ultimaker 2+, as seen in Figure 3.1.

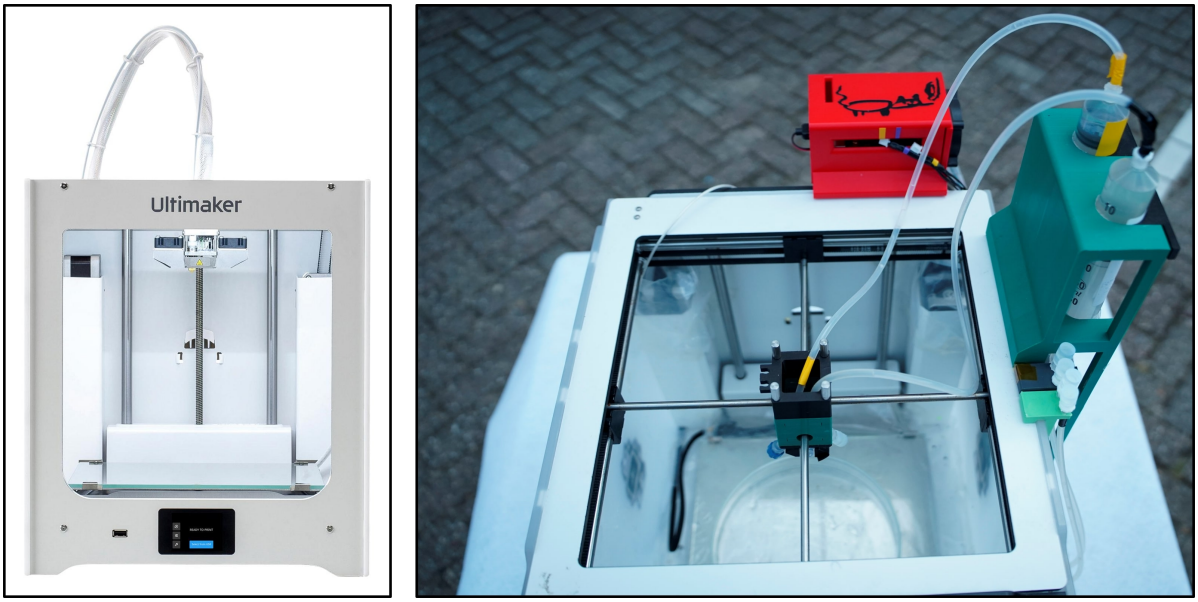

Figure 3.1: Ultimater 2+ - the building base for the modified coaxial printer (left), Gantry head assembly (right)

The UM2+ boasts a print volume 223 x 223 x 205 mm and it features a glass-bed, which coincidentally is a hydrophilic material. This is a important feature, since the resulting printed vasculatures are water-based and, thus spread on hydrophillic surfaces, which assists in slip prevention. Otherwise, the printer itself is not waterproof and is prone to rust on the gantry, so the printer was waterproofed to keep the mechanical and electrical components dry. Moreover, the printer comes with a buzzer (this was later programmed to play soothing tunes), an LED screen, and a dial to control the UM2+ LED screen software. Further, it also provides a largely walled in enclosure. This, unexpectedly, has also been a benefit that protected the surrounding electronics and surfaces from spills. All in all, this is a capable printer and a good choice as a basis for modification.

Further, elaborating on the hardware, there are a few additions to the printer. One very important addition is the dual-extruder assembly seen in Figure 3.2 (left). This extruder assembly integrates two syringes with endstops and two independent linear steppers. This, was selected to be a piston driven extrusion setup. As mentioned in chapter 2, a piston extrusion system is superior when compared to its counterparts in precision, ability to extrude viscous inks and lesser cell degradation from shear. Further, there is a gantry head assembly, seen in Figure 3.1 (right). It replaces the original printhead mount for a new one that allows for the coaxial nozzle to be mounted, and manipulated by the printer. This version of the printer also included a rudimentary coaxial nozzle, seen in Figure 3.2 (middle, right). This nozzle included a method to adjust the concentricity of the inner and outer needles by using a system of set screws, however this was not very reliable. The nozzle also could be disassembled for cleaning, even if it did take a while.

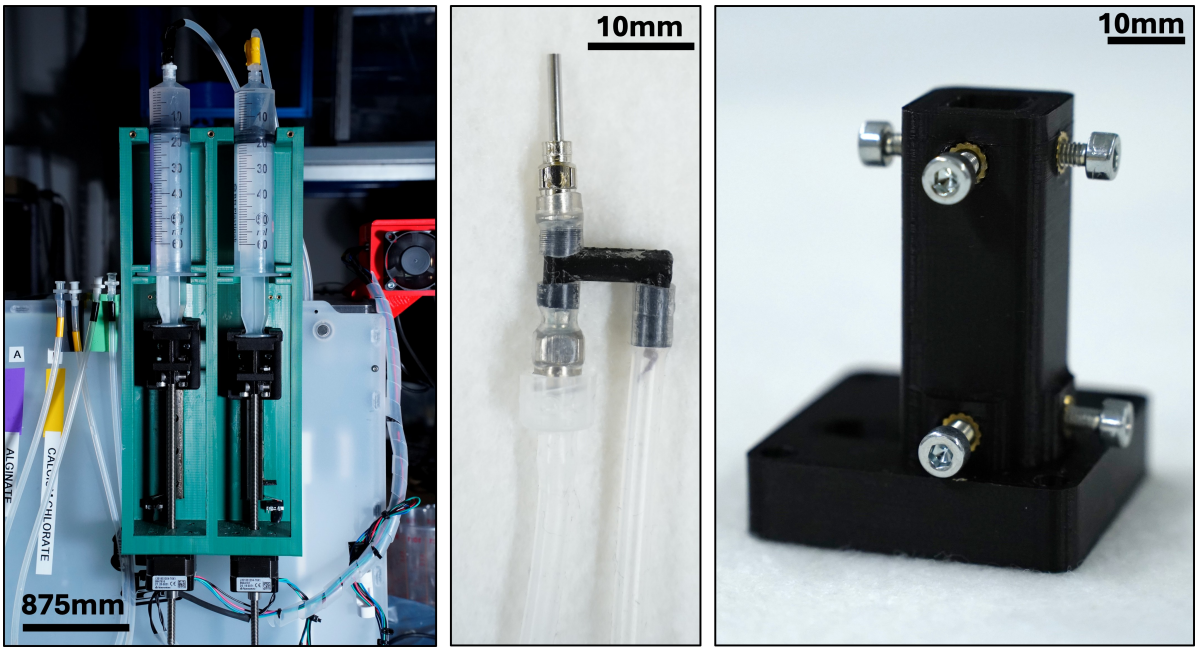

Figure 3.2: Extruder Assembly (left), original coaxial nozzle (right)

Next, the control aspects. The printer in its modified form could not be operated out of the box. This was solved using Klipper, a software used for controlling modified printers. This software was run on a Raspberry Pi 4 (Figure 3.3) which was connected to the printer mainboard and an SKR Pico . The SKR Pico is responsible for enabling the control and power delivery to the steppers in the extruder assembly. Moreover, this system utilised an inverse 5-axis control system to actuate the printer. This solution was highly cumbersome and as seen later sections, replaced.

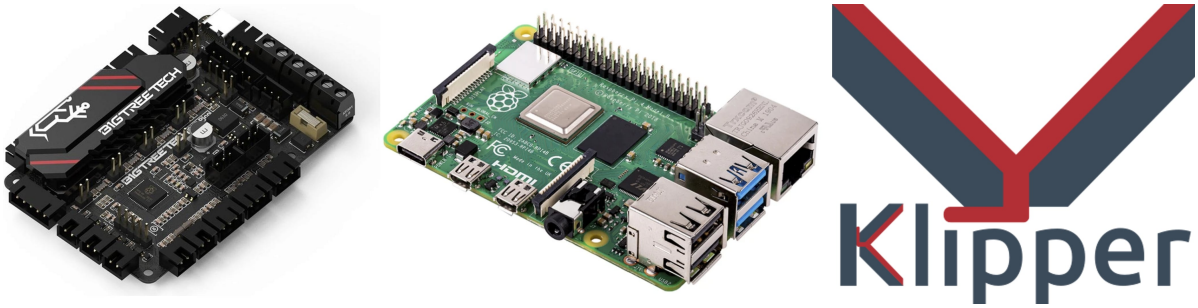

Figure 3.3: SKR Pico (left), Raspberry PI 4 (middle), Klipper, the software used to control the printer (right)

The whole initial printer system composition can be seen in Figure 3.4. The printer from this point onwards is dedicated to fusing alginate with calcium chloride, and the sticky ”shmooey” nature of the printed hydrogel has crowned it the name **Ultishmoomaker**, or USM. Additionally, the printer also goes by the name Mycocore - a play on the mycelial coreshell destinity of the printer. The USM systems subject most to change here would be the nozzle due to it’s cumbersome and rigid nature, slicing software, and additional peripherals to collect waste.

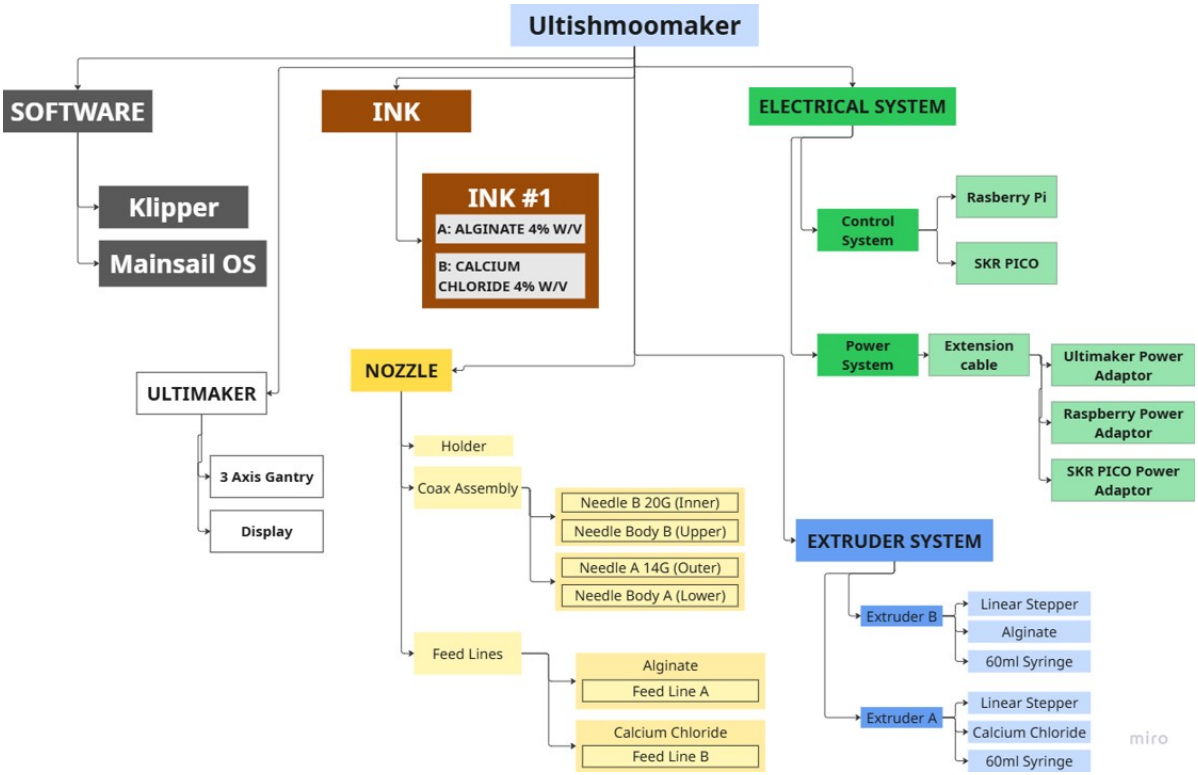

Figure 3.4: Initial printer architecture flowchart

3.3. Development

There were many developments that had to occur for the printer to reach a state of sufficient operation fulfilling the requirements. This section seeks to present the design choices and path of the final printer architecture. Here, subsection 3.3.1 will present the hardware development path and subsection 3.3.2 will discuss the software and control developments.

3.3.1. Hardware

Hardware - the stepping stone to anything physical. This subsection will present the nozzle development, as well as many of the peripheral solutions needed to print safely and reliably.

Nozzle Development

The nozzle development as mentioned in section 3.2 began with the nozzle designed by my supervisor Mark Ablonczy. This nozzle did indeed print a couple of vasculatures, but only into a bath while standing still. However, there were a few major drawbacks and hurdles with the system at hand:

- the centering solution was not very reliable.
- the nozzle was very large.
- the assembly process was difficult and time consuming.
- the protrusion of the inner needle was not adjustable.

Concentricity was of high importance thus a more robust solution was needed as the set screws were not precise enough. Next, the nozzle footprint was very large, this would not allow to print into a gel or into a dish (which was at the time desired to be tested). More, the assembly was time intensive - this is a large drawback enabling such a clog prone technology to lose lots of time in cleaning and not actually printing. Last, the relative z placement of the nozzles was important to prevent clogging - this was not available.

Thus, over the course of 4 months an extensive bout of iterations took place Figure 3.5, with evolution from older to newer going from right to left. The following successor was a 3 module printing nozzle

that threads together and has a adjustment mechanism similar to the initial nozzle. This is - the first iteration and it can be seen in Figure 3.6. This nozzle ensured the concentricity (and requirement **MYCO-DESIGN-03**) by aligning the needles through being integrated with a centered set of threads. In this setup the alignment mechanism was also improved only aligning the thin inner needle agains a set inner one. However, quickly it was discovered that using conventional printing methods this nozzle would be prone to leaking. This contradicts requirement **MYCO-DESIGN-02**.

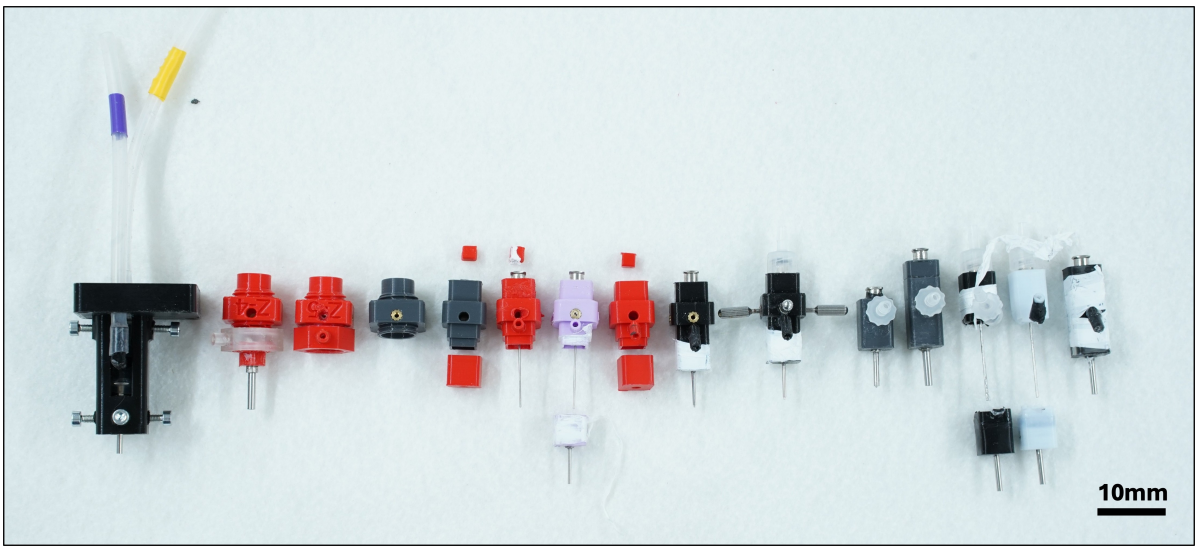

Figure 3.5: Nozzle evolution, oldest leftmost, newest right

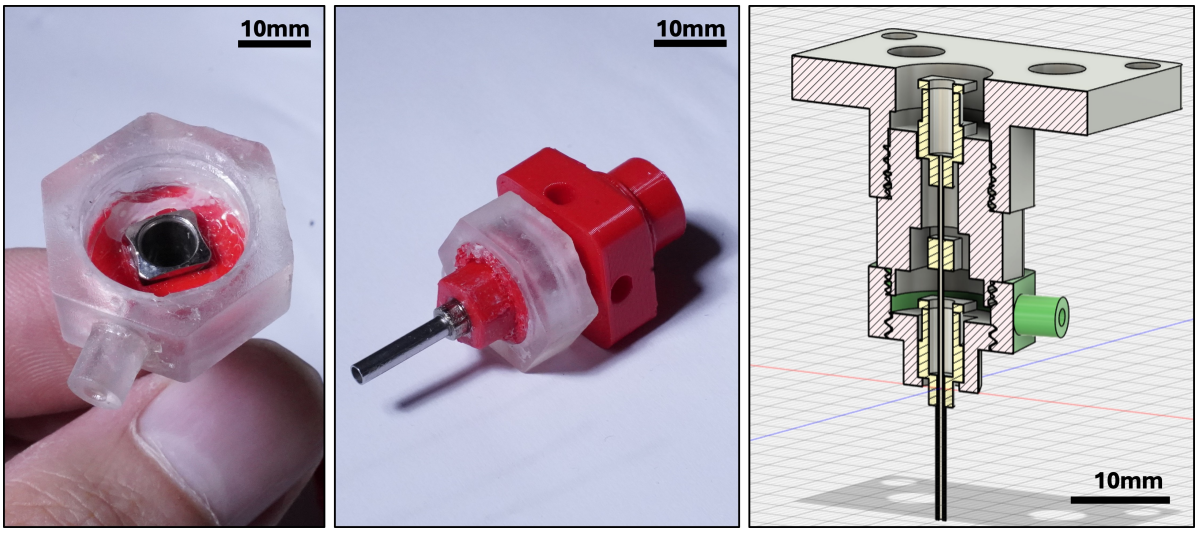

Figure 3.6: First modular nozzle (left), Middle and bottom nodes (middle), CAD model of first iteration (right)

To meet the design specifications, it was necessary to iterate the design. This is the second iteration, that was glued. Initially it seeked to retain the centering mechanism as seen in Figure 3.7 (middle), however, that too failed. The next, third iteration nozzle can be seen in Figure 3.7 (left and right). The second iteration nozzle allowed to perform many successful prints. However, it had a few severe issues. One of theses issues was that clogs were a terminal occurrence and would render the nozzle inoperable. Moreover, the nozzle was not sustainable with every part being glued together it meant that if even one of the 2 components was either badly aligned or glued in, the whole iteration had to be trashed. Additionally the inability to disassemble the nozzle would require destructive inspection to figure out the causes for a clog. This iteration did not meet requirement MYCO-DESIGN-01.

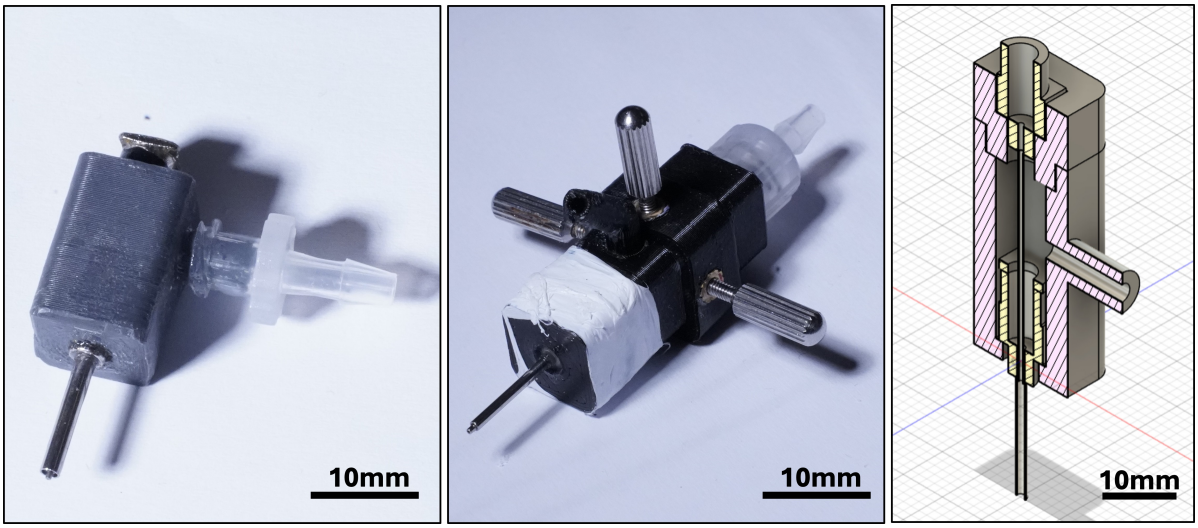

Figure 3.7: Glue in nozzle (left), adjustable glue in nozzle (middle), CAD model of the glue in nozzle (right)

The last and most successful (fourth) iteration is the resin printed luer locking nozzle. It can be seen in Figure 3.8 (left) with the cad model (right). This nozzle utilizes the luer taper system to achieve a modular, screw-together system that is modular and interchangeable. Luer locks are a type of medical connection system widely used in syringes and other medical equipment. As seen in Figure 3.9 the luer lock connection has a male and female component that have threads and an internal taper. The true genius of this system is the taper that is somewhat compliant and that makes a very tight seal once screwed in. Such luer lock fittings come in a plethora of materials, designs and applications, some of which can be seen in Figure 3.9. The luer solution allows the leaking requirement MYCO-DESIGN-02 to be met.

Figure 3.8: Fourth iteration nozzle (left), CAD model of luer-lock nozzle (right)

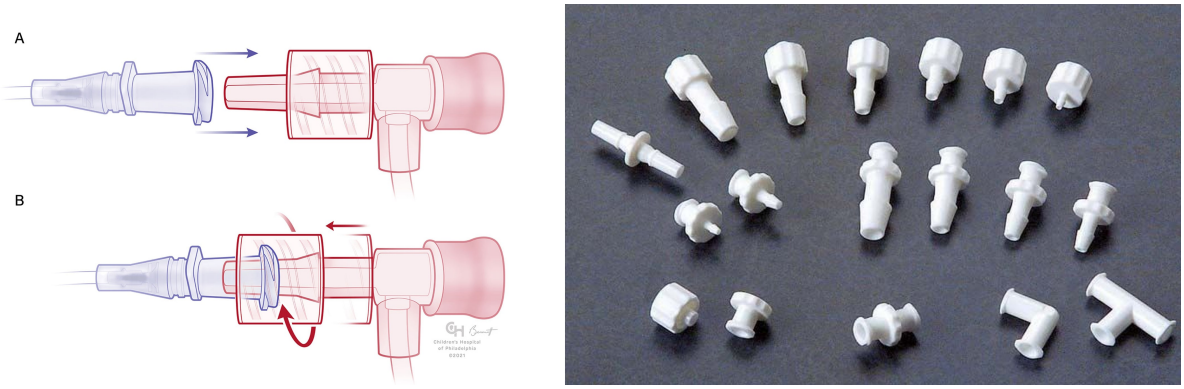

Figure 3.9: Luer lock joint concept (left) image courtesy of Anaesthesia Patient Safety Foundation, A variety of luer lock sizes and types (right) image courtesy of Hugo Sachs Elektronik

This system is also how the needles connect to the lines. By shear coincidence, during one meeting the realization had occurred to convert all connections on the nozzle to luer taper based ones. This meant not only that the system was interchangeable with many other connectors but it also made the nozzle stackable opening the possibility to have a tri, quad or even penta-axial setup with minimal changes. This completes requirement MYCO-DESIGN-01.

The design features 3 elements that make up the body (seen in Figure 3.8 right):

1. top node - containing a glued in inner needle
2. the body - the element that both the top node and outer needle screw in
3. outer needle

The top node and body are printed using a Form Labs resin printer ensuring no supports are printed on the threads and mating surfaces. Once treated the top node may be glued together. This is done assembled partially applying superglue to the top node and then manually aligning the concentricity and stick-out. Once this is done the needle is partially glued in position and can be removed to apply more glue. Lastly, before used, the nozzle should be marked to its mated top node and body (for optimal fit) and the threads and luers should be greased up using silicone grease to extend the lifetime of the nozzle.

Nozzle Holder

After the first iteration of the nozzle it was necessary to design a nozzle holder that was fast to install and remove, stiff and slender. The design of the nozzle holder followed the arc of the nozzle design since these elements are directly related. The design evolution can be seen below in Figure 3.10:

Figure 3.10: Nozzle holder evolution

The initial design was an integral part of the nozzle, and screwed in to the body. With the 2nd and

3rd iteration the holder was made to be compliant so that removal would be fast and easy seen in Figure 3.10 2nd and 3rd holders from left. A springlike mechanism proved to be too complicated (2nd holder) and not reliable enough thus, a friction-based solution was made (3rd holder). This was the correct direction, but had to be stiffened. Furhter, iterations, included openings for the 2nd iteration adjustment screws, while retaining a stiff profile. This profile was also streamlined to reduce material waste, and to make the design less cumbersome. The final design (Figure 3.10 right most holder) uses friction to hold the nozzle firmly and allows it to pop out in case a crash were to occur. Additionally, it uses heat inserted nuts so that it can be quickly removed using 4 thumbscrews. This is in line with requirements MYCO-DESIGN-01 and MYCO-SAFE

Peripherals

Alongside the nozzle development the printer received a number of peripheral upgrades. These upgrades were aimed at increasing efficiency, reliability and often to prevent damage. Additionally, many usability upgrades resulted in the ability to test, and iterate in quick succession. The first of these peripherals are the two waterproofing improvements. Waterproofing is very important in the context of this project because many spills, sprays and small water-based explosions occur on a regular basis. First is the enclosure waterproofing seen in Figure B.7. Since the internals of the printer sit below and all of the ink often purges and spills beneath the bed - a non sealed bottom of the enclosure is a very fast way to short-circuit the mainboard of the Ultimaker. The SKR Pico and Raspberry Pi are also subject to splash, thus a case was made for these as well, seen in Figure B.8.

Moreover, another key addition was the use of separate marked lines. As seen in Figure 3.5 all lines used to print and fill the syringes are color coded with light colors (yellow/white) for calcium chloride and dark (purple/black) for alginate. This is essential because an operator error when attaching, replacing or cleaning could create a clog and destroy the nozzle. This is also done with the stepper motors, end stops. Additionally, separate filling lines are used to fill the syringes, so that the existing ones do not have to be removed from the printer Figure 3.11

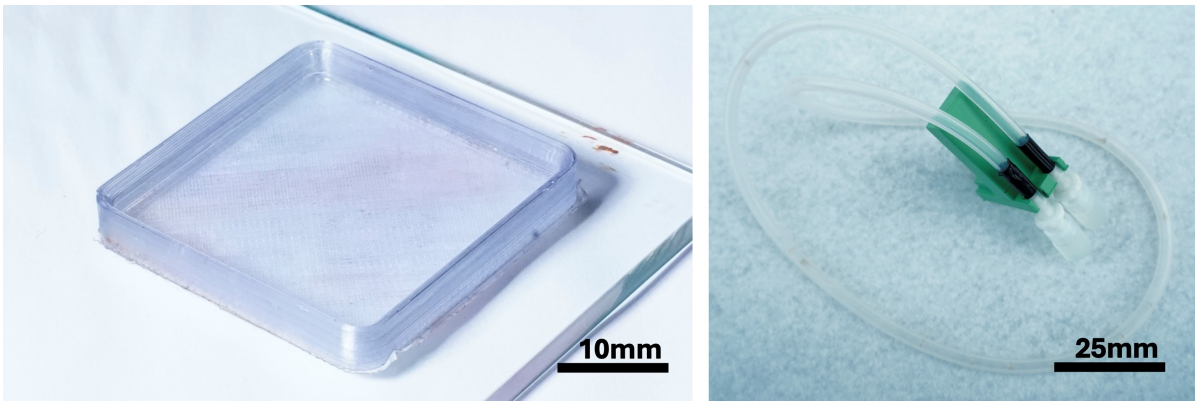

Figure 3.11: Purge bed (left), filling lines (right)

Further, a purge bed (Figure 3.11) added to capture the extruded material during the PURGE macro command (further explained in subsection 3.3.2). This prevents the bed from getting wet prematurely and allows for the best bed adhesion for the first layer.

Lastly, a EDTA bath (Figure B.6) was designed for nozzle unclogging. This was an attempt to use a solvent to degrade the clogs in between prints or user sessions. EDTA is a common anti-chelation agent that prevents various substances from coagulating. Thus, the strategy was to dunk the nozzle into a small concentrated bath in the hopes to loosen the formed alginate hydrogel clog inside. When a 10% solution of EDTA was tested on a pile of scrap prints, not much had occurred. Some breaking down of the hydrogel was occurring, but it was certainly not sufficient to make any difference in the short-term and questionably in the long term. The next step in development was envisioned to be a different, more corrosive solvent, but by now the elegant nature of the solution was lost and all developments were stopped. However, if this were sufficiently developed then the need for a nozzle that can be disassembled would not exist.

3.3.2. Software and Control

A computer numerically controlled machine requires not only hardware but supplementary software to exhibit motion and control. For this very reason this subsection will be dedicated to explaining the software suite and control system used by the bio-printer.

Klipper

As mentioned earlier, Klipper is the software used to control the UM2+. Klipper however is accessed through a tailscale connection using Mainsail OS Figure 3.12.

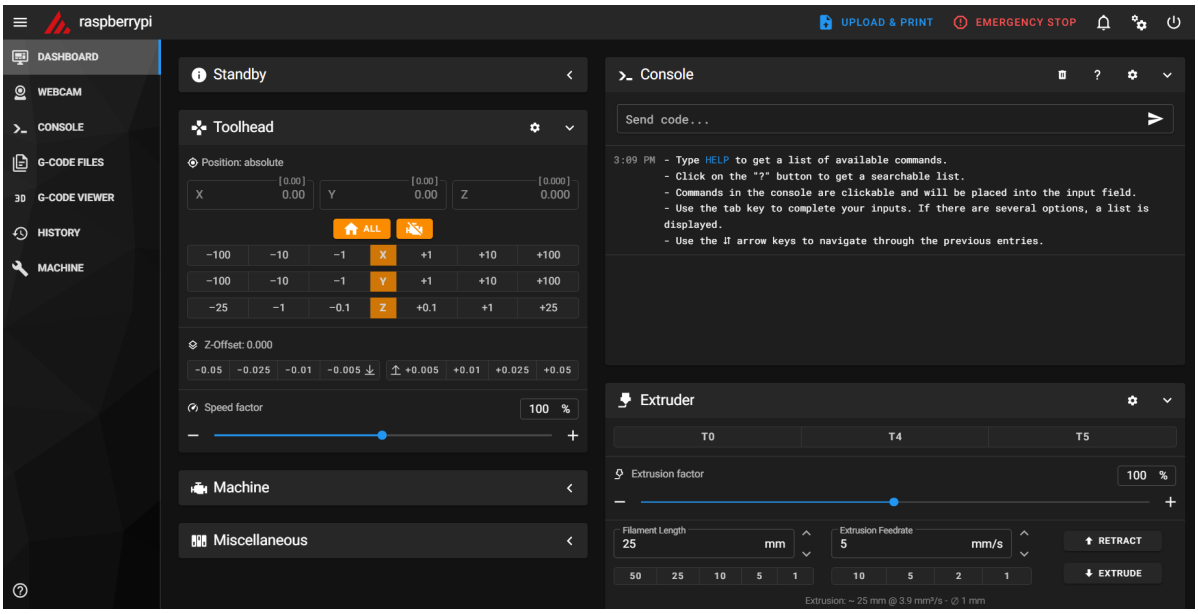

Figure 3.12: Mainsail OS environment

Using Klipper many of the printers behaviours can be configured and calibrated. One of such, very important developments was to convert the printer from the original multiple axis CNC setup to a conventional multiple extruder setup. The 5 axis configuration operated as if a 5 axis CNC machine, where a movement such as *G1 X1 Y1 Z1 A1 B1* would be executed and calculated in 5 dimensional space. Originally by using 5 axis Pythagorean theorem inversely, it was possible to infer what the effect of a certain distance in A and B (extruder axes) was. This however, would've required a completely bespoke slicer development and is not at all intuitive. However, the norm for printing fluids with pistons is a simple direct ink setup where the extruder treats the filament as the diameter of the syringe. Moreover, multiple extruder mixing printer heads exist that combine or exchange filaments mid-print. Thus, by combining the mixing head functionality and direct ink printing methods it was possible to set up the printer as a multiple extruder printer.

In addition, Klipper allows for programming of macros Figure 3.13. Macros were invaluable when setting up this printer, allowing to set up movement, status and mathematical ratio functions. Here are the key macros for operation of the printer:

1. **MIX A = x B = y** - the mix function allows one to control the set mixture ratio between the two extruders. By inputting *MIX A=0 B=1*, the extrusion of syringe A will be nullified, while B will extrude nominally. The variables A and B define what is the amount extruded as a multiplier or the nominal (G1 E1 - 1ml extruded by both syringes)
2. **PURGE** - This macro locates the print head and checks whether the head is sufficiently high enough, adjusts height if necessary and returns to the purge pad and extrudes a specified purge amount. The height avoidance function is done in case it is desired to print in a dish, and in general tends to avoid objects on the bed.
3. **HOMING A/B** - This function is used when one of the syringes is finished to home the extruder.

Once activated it runs a script that triggers the end stop as a filament run out sensor stopping the script and the extruder. It is useful to use when exchanging an empty syringe for a full one.

4. **CENTER** - moves the head to the center of the bed at at specified height. This is often used in the slicer preamble gcode after purging so that the head does not crash into the purge bed.

It is important to note that the PURGE macro is very useful to deduct whether the vasculature is vascular, as well as, a simple test when combining new nozzle pairings.

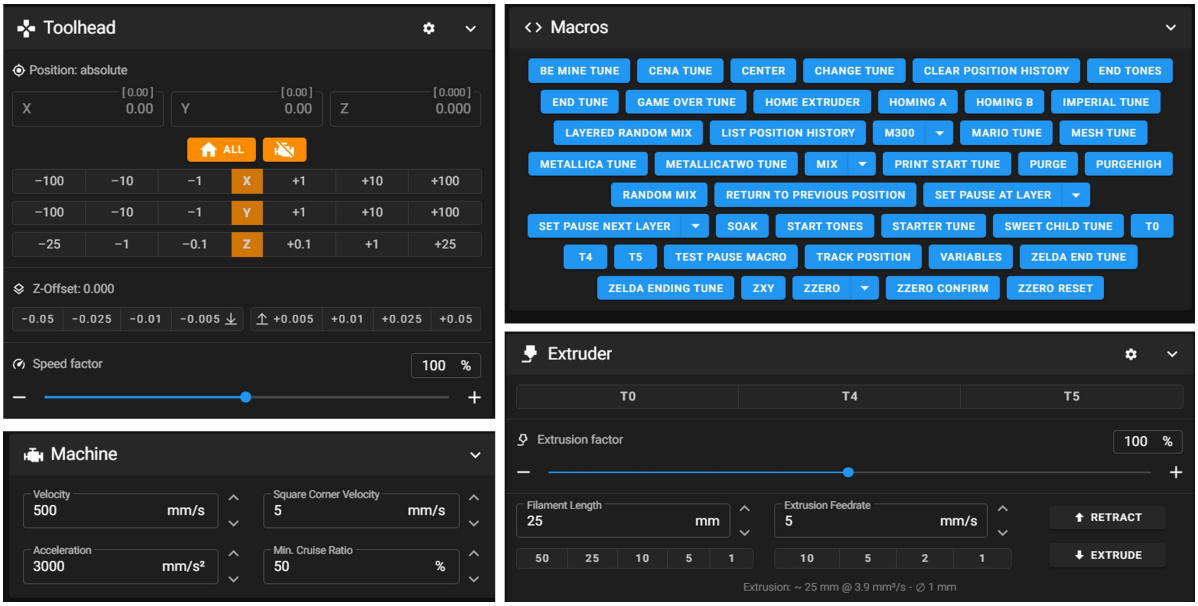

Figure 3.13: Mainsail OS menus

Slicer

One of the most important features that were introduced in terms of the printing automation process is the slicing support configuration. During this project Superslicer Figure B.4, was configured to slice specially made CAD models in a continuous filament manner. This is the ultimate quality of life improvement allowing for many 3D models to be quickly designed and printed on the spot. The method to select the correct print setting is to look for the inner needle diameter first in the first menu, then to select the optimal F400 speed and in the last menu to select, the newest iteration of the setting with the nozzle and offset parameters desired. For the nominal (described in the next chapter) nozzle this would be:

1. MycoCore - 0.8 mm, V1 - Works for Gridlet
2. Syringe, F400
3. MycoCore - 0.8 mm, G28, Z1, PERFUSION

3.4. Final Iteration

After a many considerations and additions the development of the 3D Printer could now finally come to an end. In the process many iterations have come and go and Figure 3.14 illustrates the casualties of progress well.

Figure 3.14: Discarded iterations that went towards the development of the printer

The final 3D printer iteration is as seen in Figure 3.15. The main areas of development and change are both in the hardware sense and software. Of the hardware the most notable change is the modular coaxial nozzle. As mentioned, this very nozzle in Figure 3.16 is fully modular, 3D printer in house and at least 10 times cheaper than the closest commercial option. This is the most meaningful improvement since downtime is minimised in the event of a clog, poor concentric alignment or a broken nozzle. chapter 4.

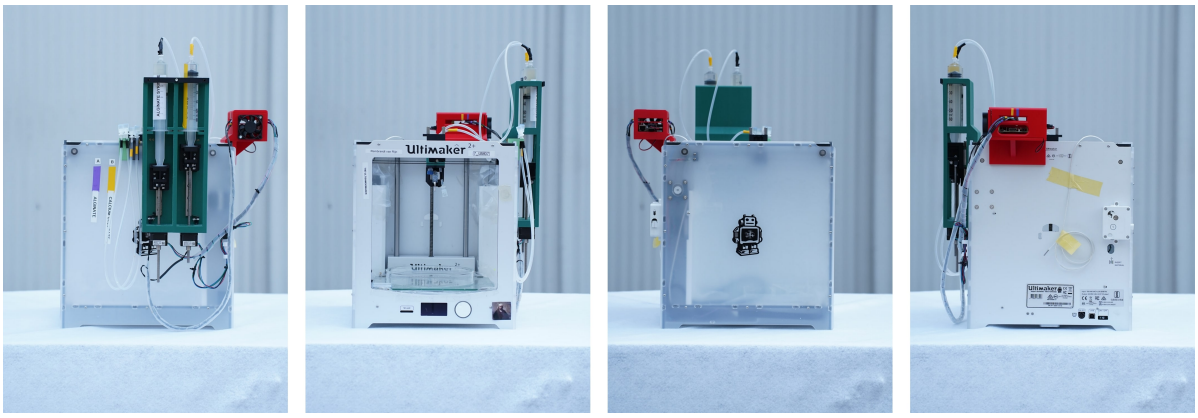

Figure 3.15: 360° view of the USM printer

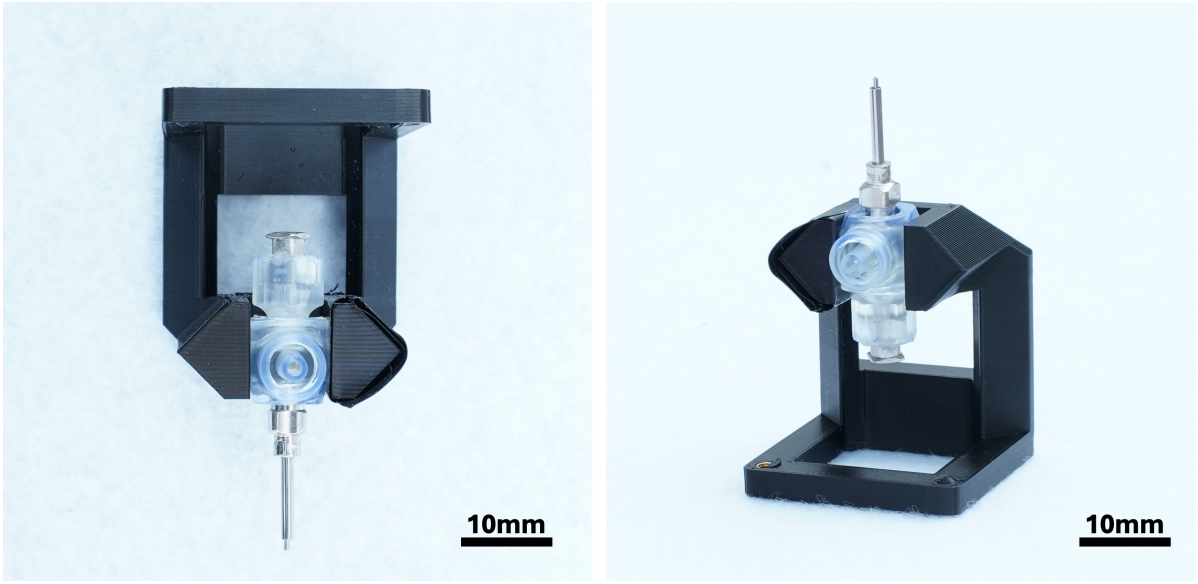

Figure 3.16: Front view of the final nozzle design (left), final luer nozzle design at an angle (right)

The evaluation of the requirements can be seen in Table 3.2 where the dark blue color indicates a completed requirement.The modular and detachable design of all elements (nozzle, lines, luer connectors, extruder module, electronics case, holder) illustrates that requirement MYCO-DESIGN-01 is met. Additionally, two more design requirements can be verified at this stage, through software implementation. MYCO-SAFE is enabled through the Mainsail environment of Klipper, where a emergency kill switch is present. Additionally, a physical kill switch is also present cutting power to the whole unit. This requirement is also reinforced through colour coding of ink related components such as the tubes, switches and stepper cables, which as stated prevents needles user error. Requirement MYCO-CAD-01 is met through the implementation of Superslicer, which enables the slicing of CAD Files. For this multiple profiles have been made so that the various nozzles could be used, as well the software has been tuned to produce continuous filament prints. Further, the fourth iteration of the nozzle mitigates leaking through luer joints and verifies requirement MYCO-DESIGN-02. This nozzle also allows for manual, on-the-go adjustment of concentricity verifying requirement MYCO-DESIGN-03. Lastly, the set of requirements that is left are related to the performance of the printer. These requirements were validated through means of testing in chapter 4. At the end of chapter 4 the complete list of design specifications are re-evaluated.

#	REQ ID	Validation Method	Verification Comments	Description
1	MYCO-PRNT-01	Test	Verified through test	The 3D printer shall produce prints capable of perfusion of 20 ml
2	MYCO-CAD-01	Review of Design	SuperSlicer can slice files In particular format.	The 3D printer software suite shall allow for slicing .stl and .3mf files
3	MYCO-PRNT-02	Test	Demonstrated the possibility to vary vasculature sizing	The 3D printer shall be able to print vasculatures of 3 different ID
4	MYCO-SAFE	Review of Design, Inspection	Waterproofing and emergency stops are present	The 3D printer shall have measures to prevent user error damage to the printer
5	MYCO-DESIGN-01	Review of Design, Inspection	Nozzle is modular, accommodates different diameter needles	The 3D printer shall have a modular nozzle
6	MYCO-INK	Review of Design	Printer has been developed using these inks	The 3D printer shall support printing in alginate and calcium chlorate
7	MYCO-PRNT-04	Test	Demonstrated through test	The 3D printer shall print perfusable planar angles with an error after the feature, no greater than 10 deg
8	MYCO-PRNT-05	Test	Demonstrated through test	The 3D printer shall print perfusable planar radii with an error after the feature , no greater than 20%
9	MYCO-PRNT-06	Test	Demonstrated through test	The 3D printer shall be able to print a perfusable structures of 4cm in height
10	MYCO-DESIGN-02	Review of Design, Inspection	Final iteration does not leak	The modular nozzle shall not leak
11	MYCO-DESIGN-03	Review of Design, Inspection	Concentricity of final nozzle achieved	The distance between the inner and outer needle walls shall be larger than 1 wall thickness of the inner needle

Table 3.2: Requirement verification table. Dark blue indicates the requirements that have been met at this point of the thesis.

4

Coaxial Printing Testing & Validation

”I have not failed. I’ve just found 10,000 ways that won’t work.” - Thomas Edison. To create a reliable base for printing vasculatures, an approach to formulate, verify and validate the process and results of printing was necessary, which is covered by this chapter. Firstly, section 4.1 presents the development of the printing process. section 4.3, section 4.4 and section 4.5 present the testing campaigns related to the validation of the bioprinter design.

4.1. Developments & Tests

All home runs are a culmination of meticulous trial, error and preparation. This section covers how the first replicable results were achieved and what events led to it. In subsection 4.1.1 the bio-ink preparation is presented, while subsection 4.1.2 covers the tuning and selection of initial printing parameters. Lastly, subsection 4.1.3 and subsection 4.1.4 present the major failures and perfusion solution development, respectively.

4.1.1. Bioink Preparation

Before any printing can occur - an ink must be made. These inks are (can be seen in seen in Figure 4.1):

1. Sodium Alginate solution 4% W/V
2. Calcium Chloride solution 4% W/V

This specific concentration was chosen from the findings in chapter 2 based on a publication that detailed alginate vasculature printing in baths. The effects of sodium alginate concentration have to do with how viscous the ink and stiff the hydrogel will be. A low viscosity fluid is easier to work with in terms of filling the syringes, which is common occurrence. However, the lower the concentration of the ink the lower the stiffness and strength of gel[2]. And with lower calcium chloride concentrations, the slower the crosslinking occurs. Having tested the 4% proposed in literature[2], the results were satisfying. Therefore, no other ink formulations were investigated.

Figure 4.1: Alginate (opaque) and Calcium Chloride (clear) Inks (left), Alginate mixing setup (right)

The preparation of these inks is straightforward and non-hazardous. Both alginate and calcium chloride are bio compatible materials and can be washed conventionally down the drain using water. Alginate is made by using sodium alginate in powdered form and mixing it with water. To accelerate the mixing of the alginate it was done while heated at 50°C and continuously stirred with a stir-bar overnight at 750 RPM, as seen in Figure 4.1. This is done while covered to prevent loss of water. Next, calcium chloride can be measured out and stirred into solution with water. This does not require automated stirring, since the calcium chloride dissolves very easily. Once made, the alginate should be refrigerated and away from UV exposure to extend shelf-life

However, during the print parameter tuning mentioned in subsection 4.1.2 uncontrollable random vasculature formation failures began occurring. It was so severe that the attempts to print line samples was scraped for a session of purging to tune the parameters. Initially this seemed to be a hardware issue possibly an environment issue (the ambient temperature was reaching 30°C, however this was not the case). The fault was caused by an alginate ink batch that had degraded after sitting for over 2 months on the shelf at ambient conditions. This became apparent once a new batch was made and the printer began working flawlessly.

In [15] it is observed how alginate chains shorten from UV exposure, among other factors. As alginate is recommended to be stored refrigerated and out of light exposure, it can be deduced that the ambient storage conditions caused the degradation of alginate in solution. A visual comparison between bad alginate and good alginate (seen in Figure 4.2) reveals that a fresh alginate is homogeneous and largely opaque, while degraded alginate is partially transparent with white precipitate collected at the bottom. The effects of using alginate that had degraded are inconsistent vasculature formation at the tip and in extreme cases it leads to a minced/mashed type of consistency lacking any structural integrity whatsoever.

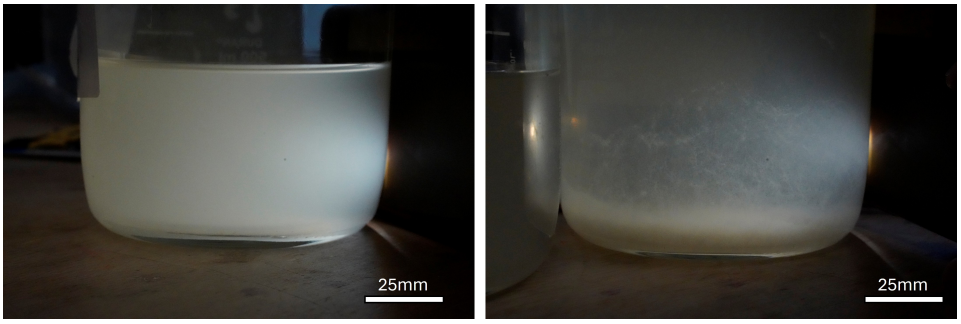

Figure 4.2: Fresh Usable Alginate (left), degraded Alginate (right)

4.1.2. Printing Parameter Selection and Tuning

With the control approaches implemented in subsection 3.3.2 and the nozzle developed in subsection 3.3.1 many variables were open for selection. These variables could be separated into two groups:

- Nozzle combination
- Printing parameters
  - Extrusion Modifier
  - Mixing Ratio (MIX macro from subsection 3.3.2)
  - F Speed
  - Printing offset

First, the needle pairing for the nozzle had to be selected. An overview of the available needle sizes is given in Table 4.1. To pair a set of needles the inner diameter (ID) of the outer needle (ON) has to be bigger than the outer diameter (OD) of the inner needle (IN).

Specifications	ID of Needle (mm)	Needle OD (mm)	Delta
10G	2.693	3.404	0.711
12G	2.159	2.769	0.61
14G	1.6	2.1	0.5
15G	1.35	1.8	0.45
16G	1.16	1.61	0.45
17G	1.07	1.47	0.4
18G	0.86	1.28	0.42
19G	0.7	1.07	0.37
20G	0.6	0.9	0.3
21G	0.5	0.8	0.3
22G	0.4	0.7	0.3
23G	0.33	0.63	0.3
24G	0.3	0.55	0.25
25G	0.26	0.5	0.24

Table 4.1: Table of needle sizes

At first glance the pairings would seem to be almost limitless and questionably useful. The intuitive selection was to select a nozzle as small as possible to achieve a resolution as high as possible. However, this is not the first time coaxial printing has been attempted and coaxial needle variants for printers already exist. The company CELLINK sells coaxial nozzle kits[1]. Nevertheless, there are some sizing effects with varying needle sizes. First, concentricity is easier to adjust with needles with a larger gauge difference due to there being more margin. Next, the smaller the needle the more restricted the flow

[1] https://www.cellink.com/product/coaxial-kit/

becomes. This, in turn, increases the pressures for the same increment of massflow, as well, increasing the pressure experienced in the lines. Moreover, due to a smaller outer area (in the alginate flowing section) a catastrophic clog can form a lot quicker and more severely. Since, as mentioned in chapter 2 coaxial printing is very prone to clogs the result of a smaller diameter (such as the ones listed in Table 4.2) is a plethora of gooey explosions, leaks and broken nozzles. Thus a gauge difference of 4 was exchanged for a gauge difference of 6 (between IN and ON). The initial CELLINK pairing sizes with the final needle pairings can be seen in Table 4.2.

	Nozzles	ONA (mm2)	INA (mm2)	Ratio
#	**Selected needle pairings**			
1	14G-20G	1.37	0.28	4.86
2	12G-18G	2.37	0.58	4.09
3	10G-16G	3.66	1.06	3.46
#	**CELLINK needle pairings**			
1	16G-20G	0.42	0.28	1.49
2	14G-18G	0.72	0.58	1.25
3	12G-16G	1.63	1.06	1.54

Table 4.2: Table of commercial CELLINK needle pairings and final selected parings

Initial Parameter Tuning

Having selected a range of needle pairings, a nominal printing parameter must be found. For this a series of purging tests and line prints were conducted. It is important to note that during these observations an alginate spoiling had occurred. Nevertheless, the purging and prints still gave great insight into the effects of the parameters on vasculature formation. Firstly, the B to A ratio was tuned. From this it was deducted that calcium chloride is the limiting variable (B) and alginate (A) is not so much. An increase of alginate (A>1) had no visible effect on the vaculature dimensions when printed on a bed. The effects seemed to be only an excess of deposited alginate, since the calcium chloride has an upper limit of material it can access for instantaneous crosslinking. However there was a lower limit of alginate to where it was no longer sufficiently abundant to form vasculatures. Moreover, calcium chloride has a lower and upper limit, as well. The lower limit is characterized by a non continuous flow causing the printing of a line of bead like formations. On the other hand, calcium chloride at B = 1.5 starts flowing too quickly and abundantly, printing in a somewhat uncontrolled fashion. During purging at B = 1.5 the usage of calcium is very large, and even if the formed vasculatures are vascular such a setting is simply wasteful and, thus can be classified as calcium chloride overextrusion. To summarize, the wining parameter was the nominal MIX B=1 A=1 for predictable and consistent results, minimizing waste.

Next, the extrusion factor (EF) was to be tuned. The ratio EF was tuned for the 1.6mm nozzle slicer setting. Starting 100% vasculature at purge was consistent and predictable, however, when printing overextrusion was occurring. Thus it was tuned for a line of 15 cm until 60% was achieved to be producing a very safe and consistent result. Further, the Z offset was tuned. Initially, with the non-tuned settings it seemed that the offset was a good thing - preventing vasculature piercing and adding a safety margin when printing. However, realistically, the cause of vasculature piercing was due to excessive needle stick-out and the Z offset was delaying the onset of over-extrusion. This was made clear in later planar tests, where the Z was set at 1.6mm - one needle diameter out to prevent clogging. Lastly, the F Speed was tuned. The constraining effects of the F speed are that, if the speed is not high enough the ink will not extrude sufficiently fast enough and the vasculature will not form then and clog. On the other hand, if the print speed is too high, the vasculature will be pierced as seen in Figure 4.3 by the protrusion of the inner needle. This happens because (as mentioned in subsection 4.1.3) the print needs to reach a steady state. After some tuning, it became apparent that F400 is a safe spot for predictable printing. This gives us a nominal set of parameters as: ***EF60 Z1.6 B=1 A=1 F400***.

4.1.3. Failed Attempts and Behaviours

In the printing process many failed prints had occurred, this subsection tries to give insight to the behaviours at hand. The first behaviour to cover would be the ”elastic buffer” of the vasculature. This so called buffer, is created by increasing the Z offset of the nozzle from the bed which forms an arc-like

filament deposition geometry from the nozzle to the bed. From observation, this buffer zone introduces elastic effects as opposed to very rigid dynamics when very close to the bed. This, in turn, makes the system compliant and allows it to stretch and correct after failure has occurred more readily. This elasticity is also one of the reasons why many bioprinting setups use alginate as mentioned in chapter 2. However, it initially also hides parameter inconsistencies (overextrusion, underextrusion), by stretching or slightly compressing, making it an undesirable property when aiming for highest dimensional precision.

Further, the needle alignment plays a very large role in the parameters and consistency of vasculature formation. As seen in Figure 4.3, the needle setup in the nozzle is so that the inner needle protrudes around 0.5mm. Otherwise, as mentioned in subsection 3.3.1 if the needle is inside the nozzle it causes severe clogging. However, on the other hand, if the needle sticks out an amount too large vasculature formation may be prevented altogether! This occurs when the meniscus of the inner wall of the vasculature is pierced when the angle of deposition is too high as seen in Figure 4.3. Thus, the limit of the needle placement for optimal performance is somewhere between 0.5mm out and 0mm (both needles are aligned). As well if the stick out is low, less offset is needed and more precise printing can be done.

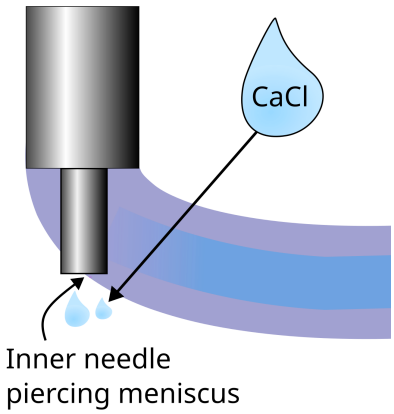

Figure 4.3: Illustration of piercing effect

Next, an important phenomena is the steady flow state. During the printing beginning the system need to reach a steady flow state, where the quality and formation of the vasculature is consistent. This phenomena is caused likely due to the compressible effects of the inks and system, as well as, pressure losses an such. For this reason purging and sacrificial lines are printed in the beginning of each print. In the early stages of the print clogs, trapped air, or bad bed adhesion, failed vascularisation may occur, however, this often ratifies itself within the sacrificial lines printed. In general, the print settings are optimised for this steady state and the aforementioned overextrusion is often not even visible until the steady state is reached.

Clogging

Clogging is another large concern. A large part of the nozzle design being modular serves the sole purpose of access in case of clog removal. Clogs may form when one ink makes it into the channels or needle of the complimenting ink. This mostly occurs if there is a plug formed at the tip of the nozzle or if the nozzle is submerged in to calcium chloride solution. Additionally after each perfusion attempt the nozzle is prone to clogging. In all of these cases alginate hydrogel forms in the orifice and creates a clog. Additionally, clogs may form if the nozzle or lines are not cleaned with water for large periods when the printer is left should not be used. This happens since dry alginate drops can easily form films and small stones that clog the system. The purging macro mentioned in subsection 3.3.2 can clear small plugs and clogs. However, in some cases it is necessary to disassemble the whole nozzle.

4.1.4. Perfusion Development

Requirement MYCO-PRNT-06 stated in Table 3.1 is to be able to print perfusable structures. To achieve this an alginate piercing block concept and a nozzle perfusion technique was developed.

Alginate Block

The alginate block was devised to be a simple way to simplify the perfusion process by hand. Originally, the first perfused prints and vasculatures were perfused by hand, by carefully piercing a vasculature and sealing the puncture with a finger. This proved to be highly unreliable and would often ruin the vasculature itself. This was not a suitable solution. Thus, the main concept was to provide a large and clear block element that could be confidently pierced with a syringe and would seal against a substantial amount of pressure. To achieve such an interface the mould seen in Figure B.2 was designed to cast alginate around an existing vasculature connecting to a print. Since alginate would be used in the casting, the block would form a crosslinked bond with the vasculature, creating a seamless and highly reinforced interface. Thus, a prototype was made by SLA printing a silicone mould. Then multiple attempts were made to cast alginate and calcium chloride resulting in castings as seen in Figure B.3. Sadly, the resulting blocks were opaque, oblong and non-entirely homogeneous. This was due to the crosslinking nature of the two inks, creating a round blob due to surface tension effects. Ultimately, this was a failure, but could possibly be innovated by using a premixed low concentration mixture of the two inks, however, this would be not very practical time wise.

Eureka - Nozzle Interface

The nozzle interface concept is the successor of the alginate block. This concept is based on using the existing vascular connection for perfusion, can be seen in Figure 4.4. Simply put, this connection is ”maternal”, naturally integrated to the process, resulting in the highest quality connection possible. Importantly, the nozzle uses common luer lock connections, thus to swap the fluid perfused is as trivial as screwing in a luer tip in to a syringe.

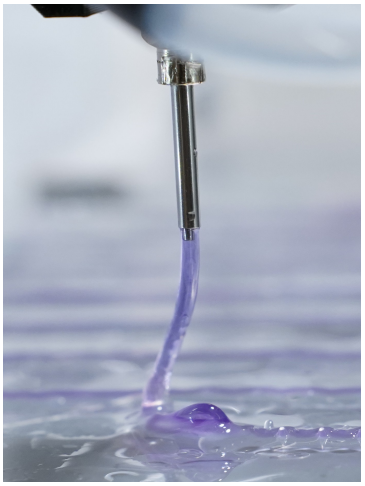

Figure 4.4: Nozzle interface

To achieve perfusion after the print is finished, one must apply calcium chloride to the vasculature-nozzle interface and (in higher pressure applications) may reinforce it by dripping additional alginate and calcium chloride interchangeably, to build up a stronger interface. Notably, this method does not fail before the actual print does, allowing for extensive testing and applications!

Microscope & Concentricity

Another important aspect of vasculature formation is the concentricity of the needles (concentric needles can be seen in Figure 4.5. If concentricity is not present then the inner channel of the vasculature cannot form. Due to the nature of the mass manufactured needles the alignment needs to be adjusted manually. For this purpose a for small needle sizes a microscope can be employed Figure 4.5, however with the nominal 14G-20G pairing it is easy to do so by eye. This is done by removing and manually

bending the inner needle for the desired effect. It must be mentioned, that concentricity does not need to be perfect in this case, due to the larger gauge difference between the needles, however the same cannot be said for tighter tolerance pairings like 16G-20G, etc.

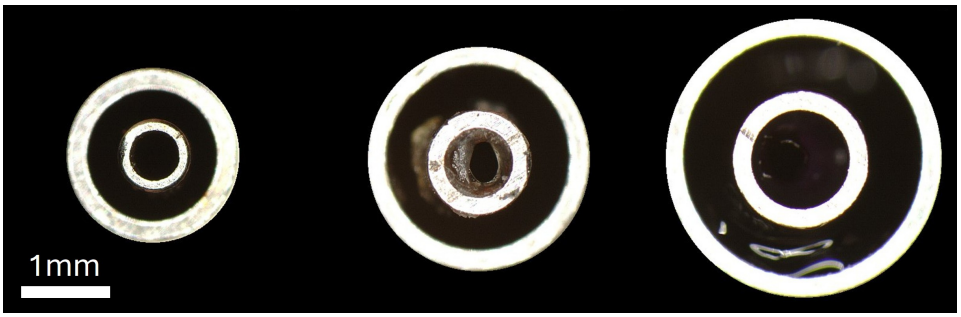

Figure 4.5: Perfect concentric arrangement of inner and outer needles

4.2. Printing Protocols

To print effectively there is a nominal protocol to ensure maximal success. This protocol can be seen in Figure 4.6.

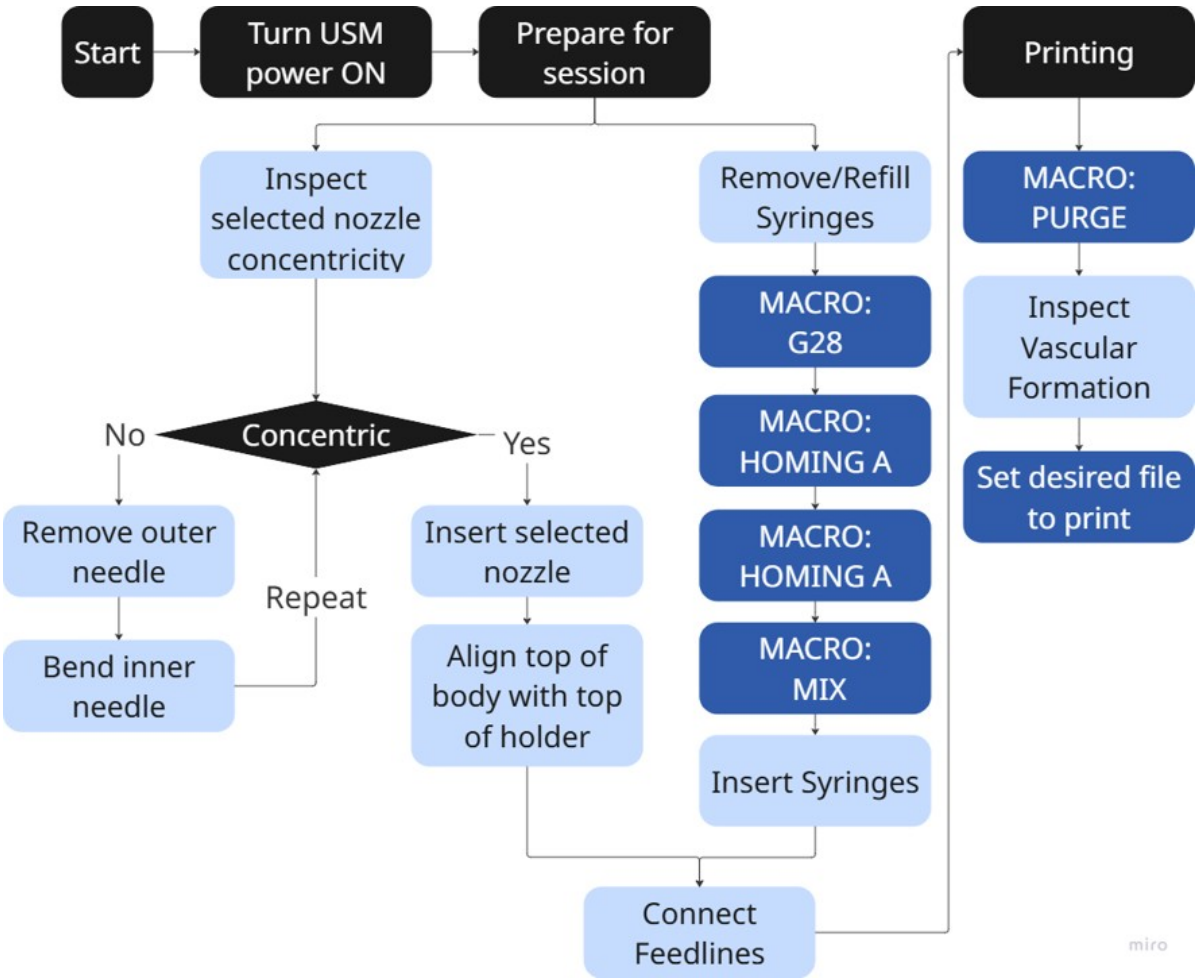

Figure 4.6: Printing protocol flowchart

The printing protocol ensures, that a person who has never seen the USM can print vasculatures

or other bioprints successfully by following the simple flowchart provided. One point omitted is the occasional need to ensure bed adhesion for the first couple centimetres by hand. This is done simply by collecting and pressing the sliding clump from the tip of the nozzle to the glass bed. This is usually followed by adhesion of vasculature and can be left to continue on its own. If all is done correctly, the user should see vasculatures such as in Figure 4.7 (left). If cut open, it can be observed in Figure 4.7 (right) that a lumen has formed indicating successful vasculature formation.

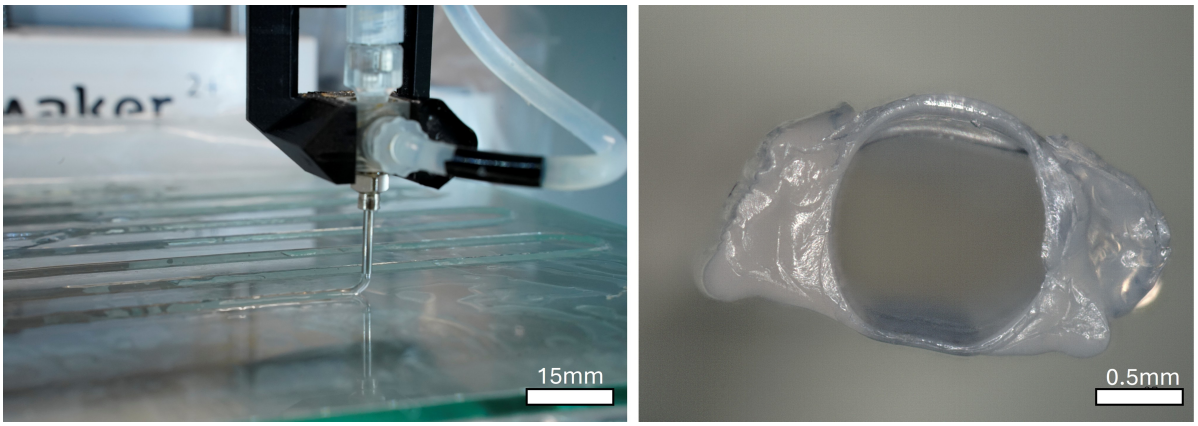

Figure 4.7: Example of a vasculature printing (left), crossection of vasculature (right)

4.3. Line Printing Test

The control of the defining parameters of a vasculature is a very desirable ability when it comes to the perfusion and construction of ever-larger, smaller structures with novel geometry and surface features. For instance, on vasculatures inside a fungi house brick (a future where walls are alive) would be preferred to be robust and large for large mass-flows of nutrients. On the other hand, an alginate gauze for treating burn victims (that would perfuse medicine) would need to be printed of small diameter vasculatures and perhaps meandering to increase the rate of nutrient delivery. Thus, in order to validate the ability of the USM to print vasculatures of varying sizes and features the **line printing test** was devised.

The goal of these tests was to quantify the effects of the extrusion factor and different needle pairings on the vasculature formation, features and geometry. However, before any of this could be done, it was paramount to quantify the extrusion behaviour of the USM. This was done by comparing the actual extruded amounts to the theoretical expected amounts.

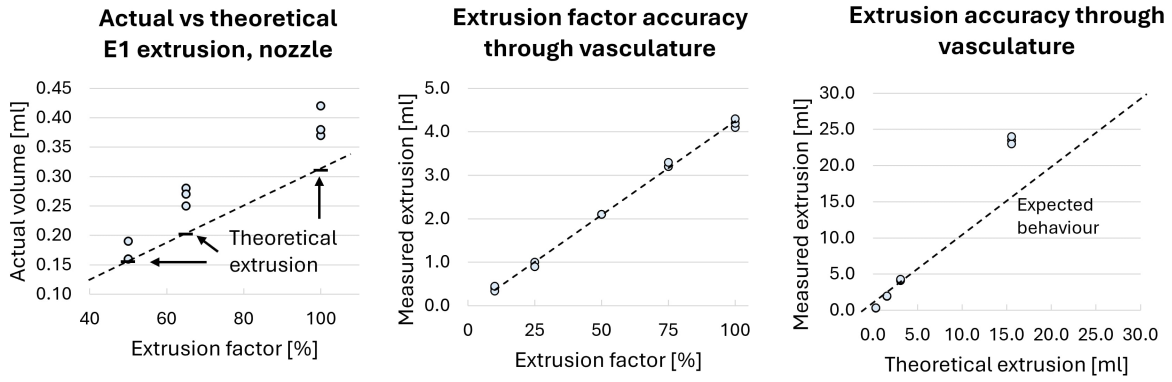

Figure 4.8: Extrusion calibration test graphs

First, the effects of the extrusion factor through the nozzle were quantified, the results can be seen in Figure 4.8. E1 refers to the *G1 E1* gcode command, which was used to extrude a single unit (relating

to 1mm of movement on the extruder). Moreover, this command has a global modifier EF (extrusion factor), which allows for the tuning of the relative amount extruded (0% - none, 1000% - 10x nominal). The expected behaviour is depicted with the dashed line, and should be a linear relation, such as Equation 4.1, here EF is the extrusion factor and $E1_{EF}$, $E1_{100\%}$ are the extruder distances with the subscript as the EF:

$$E1_{EF} = EF \cdot E1_{100\%} \tag{4.1}$$

$$E1_{100\%} = \frac{S_{2\pi} \cdot a}{b} \tag{4.2}$$

$$V_{E1_{EF}} = EF \cdot E1_{100\%} \cdot A_{syringe} \tag{4.3}$$

The nominal extruder distance is calculated as in Equation 4.2, where $S_{2\pi}$ is the stepper steps per full rotation, a the stepper rotation modifier from klipper (for tuning and b the steps/mm, a factory stepper parameter. This results in the theoretical extruded volume $V_{E1_{EF}}$ Equation 4.3. From Figure 4.8 it can be seen that the resulting EF behaviour is linear, and closely grouped for each measurement. Otherwise, there is an error that increases with extrusion factor and is more than the expected. This could be attributed to momentum effects as the extrusion is sharply stopped and the liquid inside is still moving. Moreover, when the extrusion is finished there is dripping that occurs that is due to air entering the nozzle, which allows a tiny amount of ink to escape. Nevertheless, this experiment illustrated the linear behaviour well and validates the use of interpolation to infer the extruded amount based on EF.

Further, the same test was repeated but now through a vasculature. The Bedzag print Figure B.1 was perfused into measuring cylinders to quantify this test. The middle and left graphs depict the findings, presenting the EF relation validation volume comparison of larger extruded volumes. The EF vasculature accuracy graph shows a linear relation indicated by the dashed line, that is even more accurate to the theoretical than the nozzle extrusion result. The difference between the nozzle and vasculature result is most likely due to the vasculature opening being narrow and long allowing the fluid perfused to stick better to the channel preventing dripping. Further, the expected behaviour for larger extrusion volumes is linear, depicted by a dashed line. Here the extrusion amounts were: E1, E5, E10 and E50 at 100% EF. A linear relation can be seen for the first 3 data groups. The largest extrusion amount shows an error, this may imply that the extruded amount is perhaps a more steep linear relation from errors in the software or hardware setup, however, this still concurs many of the expected behaviours. To summarize, the effects of EF and extrusion amount are linear on and predictable when compared to the theoretical, regardless of whether the volume is extruded through the nozzle or perfused through the print. Next, the effects of EF on vasculature formation will be investigated.

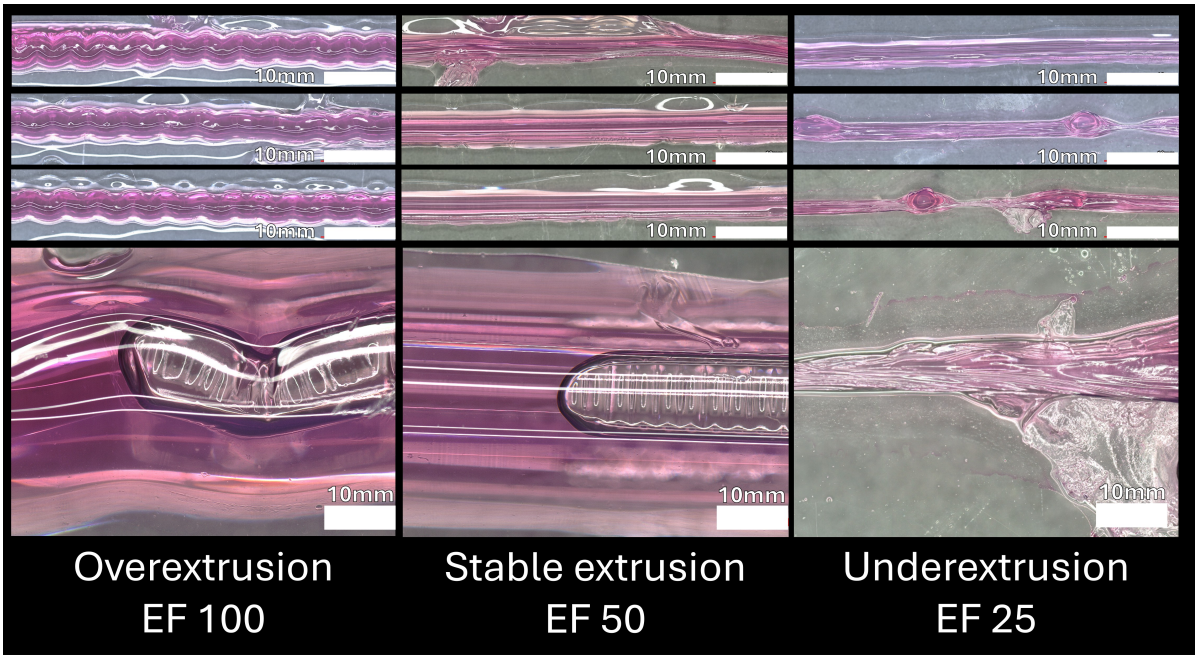

Figure 4.9: Over-extrusion, stable and under-extrusion effects on vasculature formation

Figure 4.9 shows a vasculature extruded at EF100, EF50 and EF25. In the middle the nominal stable vasculature formation can be seen - the channel is straight, vascular and perfusable, the latter illustrated by a perfused bubble inside of the vasculature. Next, over-extrusion can be seen at EF100 on the left. The vasculature exhibits a meandering, periodic formation, which is consistent and replicable. At first glance the channel can be observed to seem be larger in diameter, as well it is vascular and perfusable, similarly indicated by the artificially introduced bubble.

Lastly, the rightmost column shows under-extrusion at EF25. Under-extrusion behaviours exhibit no vascular properties, inconsistent clumping. This is most likely due to a severe lack of material w.r.t. the speed at which the vasculatures are printed. Moreover, at low EF the vasculature may fail due to the inner needle piercing the meniscus as seen in Figure 4.3. In summary, Figure 4.9 illustrates that the formation of meandering, stable and closed features can be controlled simply modifying the EF. This is a desirable feature since the closing of vasculatures could be introduced automatically. Moreover, meandering features could be particularly advantageous in applications that require a maximized surface area, like contact lenses with medicine.

With the following capabilities of the printer in mind, the next research objective was to validate that different size nozzles can produce vasculatures of varying sizes. For this the three nozzles seen in Figure B.1 and Figure 4.10 were used to print vasculatures of 3 different sizes.

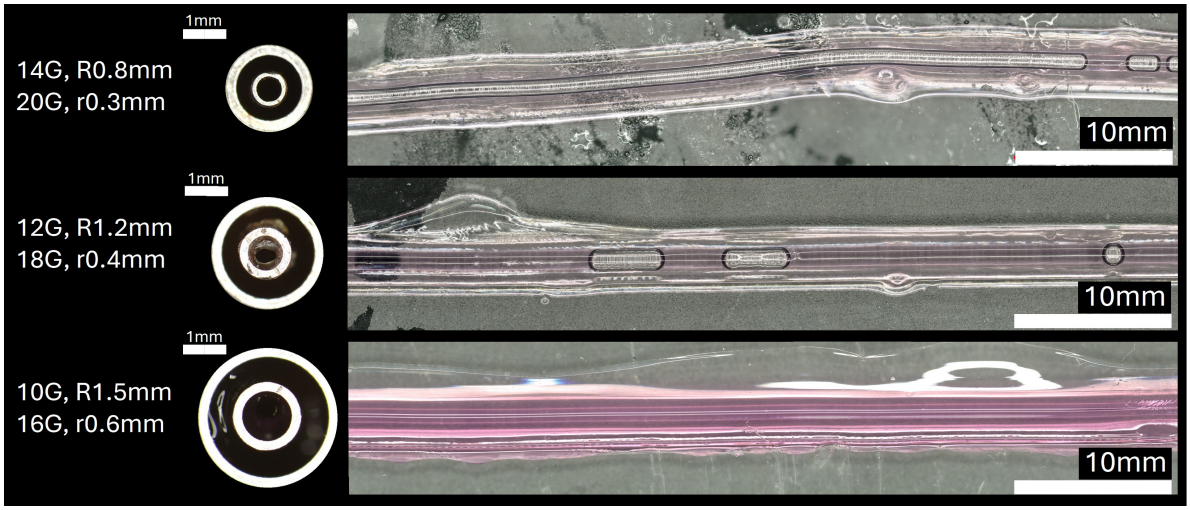

Figure 4.10: 3 nozzles used with the respective vasculatures

At first glance the vasculatures in Figure 4.10 appear to indeed be of different sizes. However, to quantify this it was necessary to measure the geometric properties of the channel. To recap, the vasculature formation process during printing can be seen in Figure 4.11. As the nozzle is extruding the two inks meet and crosslink, by creating an ”egg-box” (seen on the right of the image[16]) ionic bond between A calcium ion and the alginate molecule chain, creating calcium alginate which is the non-soluble hydrogel forming the shell of the vasculature. However, as seen in the left part of the image the alginate only crosslinks on the inside and therefore the OD (outer diameter) is not crosslinked or well defined. For this reason the goal of these experiments is to measure the inner diameter.

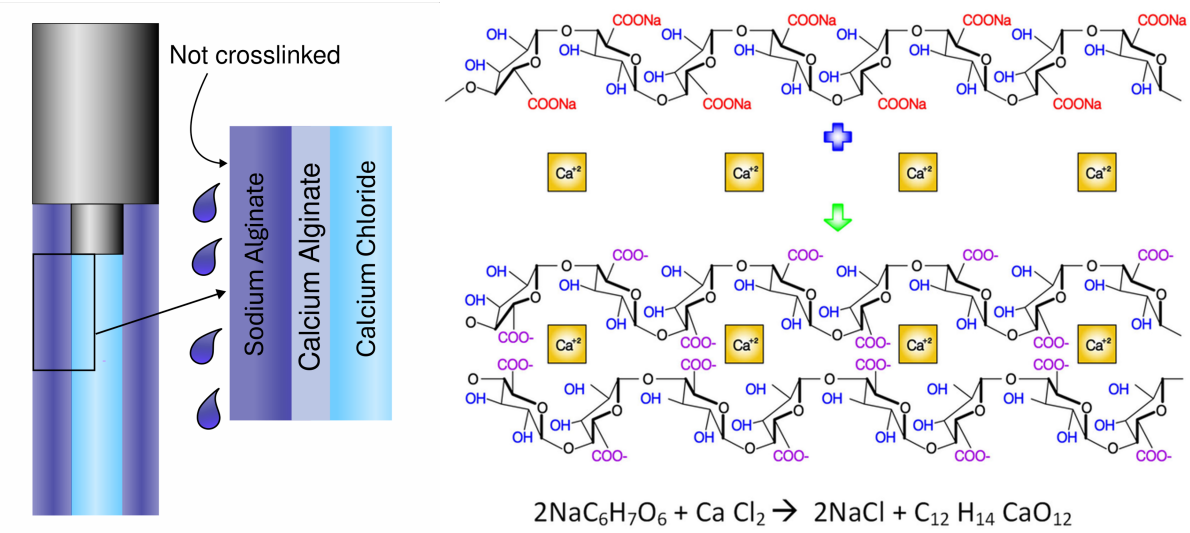

Figure 4.11: Vasculature formation at the nozzle (left), Calcium alginate crosslinking process (right) [16]

Moreover, for this reason it was theorised that the OD and ID of the IN would then determine the ID of the vasculature. Having this in mind two methods were used to measure the inner diameter, microscopy and volume measurement.

4.3.1. Volume and Microscopy Experiments

First, microscopy. When printing the transparent hydrogel there are optical indications of the inner shell formation. This can be exaggerated by printing with a dark and vivid dyes in the calcium chloride. However, when examining the vasculature under a microscope many reflections, as seen in the bottom

vasculature Figure 4.10, occur due to the wet and round nature of the vasculature. Moreover, due to the porous nature of the hydrogel the dye perfuses into the gel, painting the whole vasculature. However, by inserting a bubble into the channel manually as seen in the other two extrusions in Figure 4.10 the cavity taken up by the bubble can be then measured. More so, the lines indicating the channel walls on the vasculature segment besides the bubble can be match and identified to remove the necessity of the bubble. Using the bubble method the inner channel walls could then be measured.

Second, to verify and further validate the inner diameter measurements from the optical method a volumetric approach was devised. Assuming the inner channel is a perfect cylinder (Figure 4.12 top right figure), a known volume could be extruded into the vasculature and then it's length l measured to retrieve the inner radius, by applying a simple volume calculation Equation 4.4. Here r is the average channel radius, l measured length, V_{cyl} volume of extruded cylinder of fluid.

$$r = \sqrt{\frac{V_{cyl}}{l \cdot \pi}} \tag{4.4}$$

Thus, by inserting a bubble in the vasculature, perfusing it with a known volume, two markings were made to mark the distance the bubble travelled. The results of both both the microscopy and volume measurements can be seen in Figure 4.12.

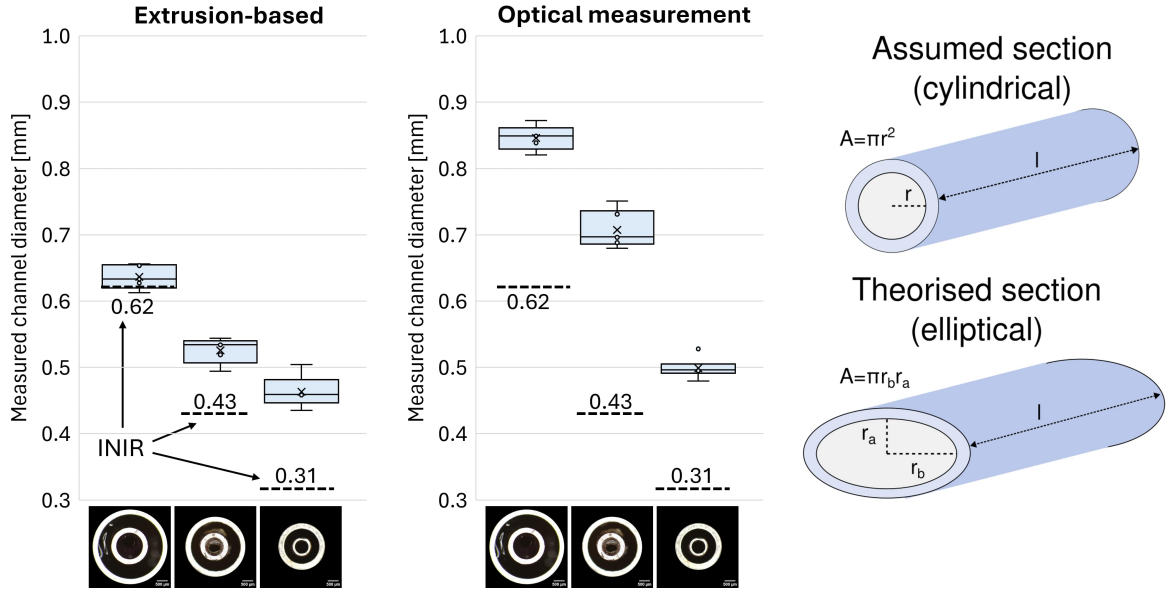

Figure 4.12: Box plots of nozzle size effect using volume method (left) and microscopy method (middle) measurements, with illustration of assumed and theoretical vasculature (right)

To begin with, it is expected that a decrease in the IN IR (inner radius) would result a decrease in the IR of the channel. It can be seen that as the nozzle size decreases so does the measured IR of the channel, as expected for both extrusion-based and optical measurements. What is more, in the extrusion-based part the nozzle 3 channel is very close to the INIR, while nozzle 2 channel is between the INOR and INIR and the nozzle 1 channel is even larger than the INOR. This indicates that the calcium chloride fills the volume that the IN takes up and in some cases goes past it. Perhaps, there are larger pressure losses with the more viscous alginate relative to the calcium chloride and as then nozzle becomes narrower the effects become more pronounced. However, the optical measurements give a much larger error when compared to that of the volumetric method. This discrepancy could be explained by the channel cross-section being elliptical. Thus, a theoretical section size could be drawn by using Equation 4.5, where r_a is the minor axis, r_b is the major axis and A is the area of the ellipse.

$$r_a = \frac{A}{\pi \cdot r_b} \tag{4.5}$$

Therefore, in Equation 4.5 the area from the volume measurements can be calculated and the optical measured radius as r_b, which gives r_a of 0.44mm for the 10G-16G pairing (largest). The elliptical shape is most likely due to sagging caused by gravity.

4.4. Planar Printing and Curvatures

The ability to print planar shapes with various features like sharp angles and large diameters is a highly desirable function. This function allows the creation of vascular meta-materials that could vary in surface area, perfusability or other material properties. But most of all, it is paramount for printing layered 3D perfusable structures. Thus, in order to validate the ability of the USM to print contours of replicable and precise parameters the **planar printing tests** were devised.

The first of the series of experiments is the L test. This experiment seeks to quantify the accuracy of printing elbow features with a sharp angle. For this 3 angles were selected 135°, 90° and 30°. These angles represent common sharp, square and blunt angles, that would be found in everyday objects. The L shapes of the 3D models can be seen in Figure 4.13, here the top section is the actual angle and the bottom meander is to reach steady vasculature formation state.

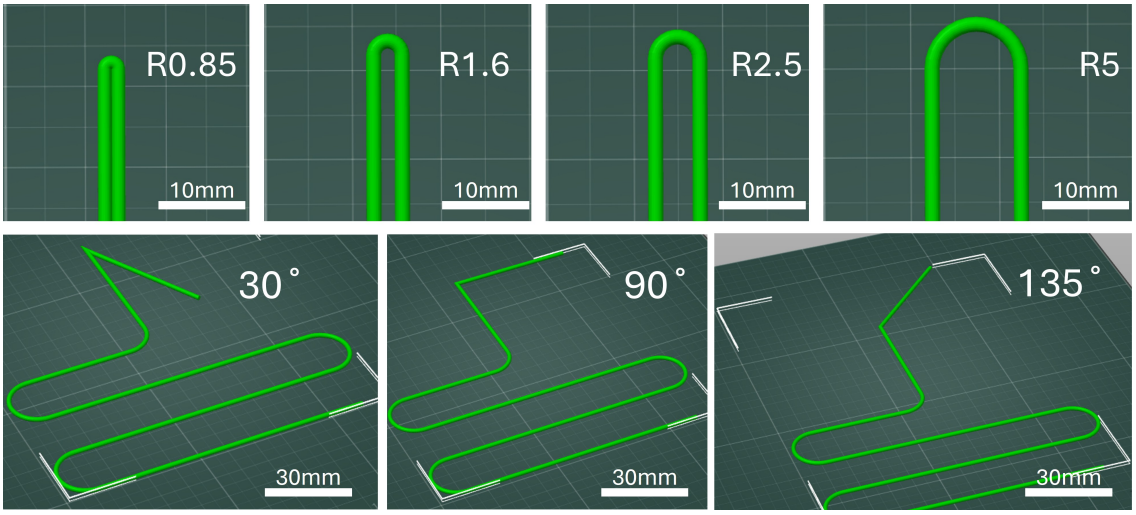

Figure 4.13: 3D models of the L (bottom) and U sections (top)

An example print can be seen in Figure 4.14. These prints were then captured from above and measured using the 5mm grid as a reference. The results of the test can be seen in Figure 4.14. Here, two sets of measurements were conducted for each sample, a measurement of the inner and outer angles. The inner angle was measured 1cm from the apex of the corner while the outer at 3.5cm. This was done to quantify the behaviour close to the feature and further way. The expected theoretical behaviour is a line that tracks the sliced path exactly.

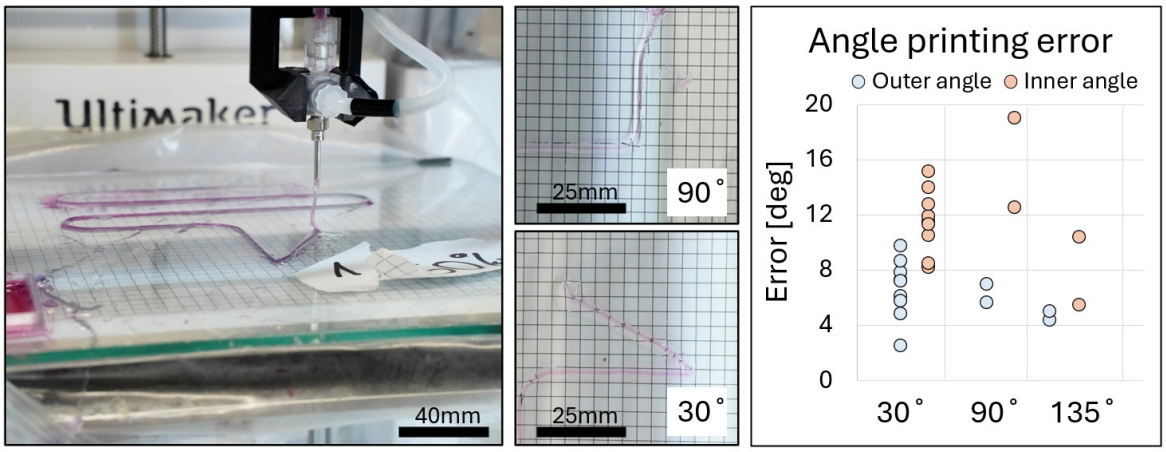

Figure 4.14: L shape of 30° on the bed (left), Top down views of angles (middle), Angle printing error graph (right)

The 30° sample was printed most since it was considered originally the most critical feature due to the sharpness of the angle. The results indicate that for all measurements the error is positive (indicating an angle larger than the theoretical). The error in general, is likely due to stiffness of the channel wall, splaying out the corner. Since the printer is laying formed filament, the vasculature, thus is not as melted PLA in traditional FDM and has a displacement and internal stiffness. Further, it can be observed that the error of the outer is generally lower than the inner angle. This indicates that the error is caused by the feature and is therefore largest there, as well as, attenuated further down the print.

Next the effect of printing on U shapes was quantified. This was done in order to understand the capability of printing radii and round features. For this experiment 4 radii were selected: 0.85mm, 1.6mm, 2.5mm, 5mm measuring from the centre to the print path of the vasculature (the middle) Figure 4.13.

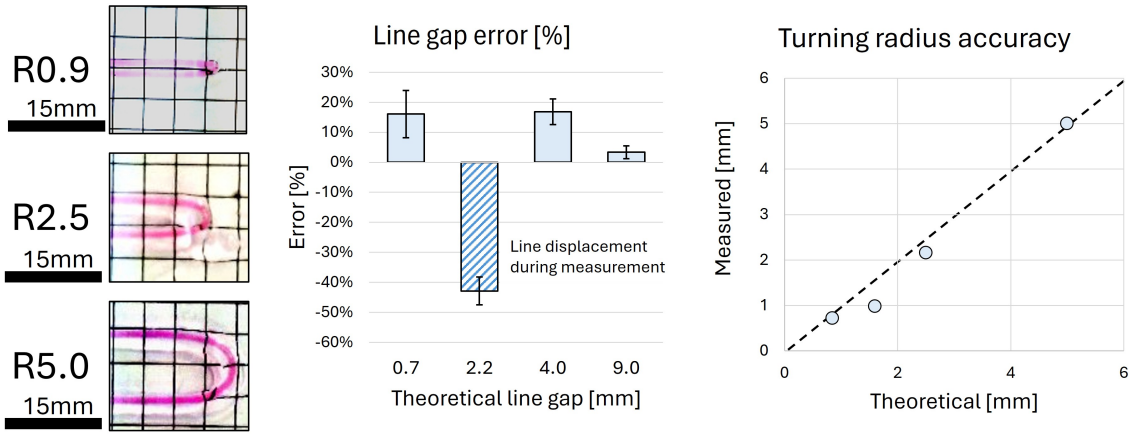

Figure 4.15: Measured prints (left), Error of the line gap (middle), Accuracy of the turning radius (right)

Some of the printed examples can be seen in Figure 4.15. For this experiment similarly for the L test, two locations were measured to quantify the effects at the feature (turning radius) and further away (line gap) from it. Here the line gap is the distance measured between the two coloured sections. The results in Figure 4.15 indicate that some error is present. The measurement for the 1.6mm radius with a theoretical gap of 2.2mm was later dismissed since it was significantly affected while handling. However, for the remaining measurements the error is acceptable and adequately low. Additionally, the error can be observed to reduce as the distance is increased this is possibly due to the non-crosslinked alginate pushing the vasculatures apart, when the vasculatures are close together. When looking at the relevant vasculatures in Figure 4.15 the wetted area is especially visible bin the specimen marked

R5.0 (lowest error), below the top part of the vasculature. This illustrates that if the excess alginate has area to deposit, the error is reduced.

Next, the measurements at the turning radius could be taken. The graph shows that the radius measured behaves in the expected linear behaviour (dashed line Figure 4.15) and follows it relatively closely. However, contrary to the linegap results, the error on average is negative (indicating a smaller radius). A smaller radius at the feature could be explained by the fact that as the feature is printed, the vasculature is slightly is pulled in - reducing the radius. Both results show, that the error is relatively small, consistent and replicable validating the ability of the printer to print such radial features.

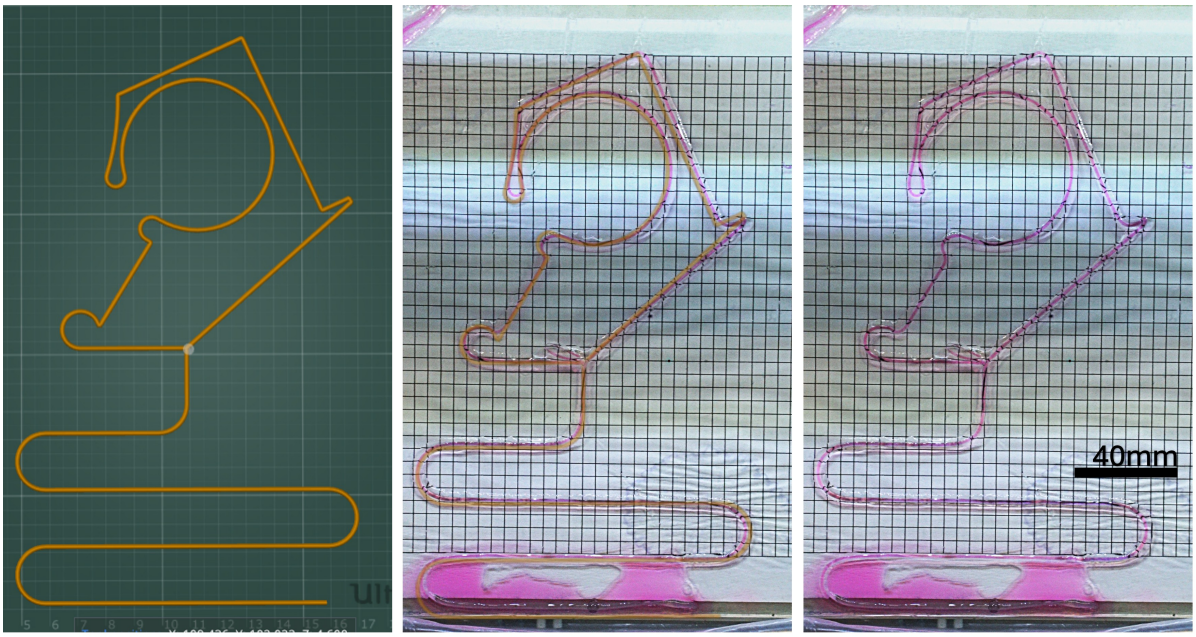

Figure 4.16: Limit course overlay. 3D limit course model (left), Model overlay over measurement (middle), actual print (right)

Finally, the full planar printing capabilities could be validated. The final test is the planar limit course test. This test was devised to combine various harsh features in a complex contour to verify whether the USM performs as intended. The limit course alongside the printed sample can be seen in Figure 4.16. The resulting sample follows the contour closely replicating even the sharpest of corners. However, some splaying, rounding effects can be observed and some sections are attracted by Van der Waals forces. This, can be explained by the effects previously discussed in this section. Notably, this result is consistent and replicable which implies that truly 3D layered prints are easily attainable. Lastly, the inaccuracies could be ratified by additional tuning and a reduction in nozzle sizes, which would reduce the stiffness effects relative to print size.

4.5. 3D Printing

The final frontier - fully perfusable 3D prints. The level of control and precision for fully perfusable 3D structures, is the main goal of the design and execution of this thesis. Printed custom substrates for fungi electrodes, on the spot printing of whole arteries, and many more applications rise from the ability to print up. Thus, in this section the final validation points for the USM will be presented. For this a bridging test and 3D demonstrator prints were carried out.

First, the bridging test. This test aims to quantify the bridging capabilities of the USM. Bridging is the printing of material across a gap with no support below. Since the USM prints its filament continuously to retain perfusability, supports that are not integral to the vascular network are not possible as of the current. However, if sufficient bridging is possible, then many supportless structures become attainable.

To test the bridging capability a series of the bedzag print from Figure B.1 was printed over two combs of 5mm height, and with gaps of up to 30mm and 40mm, as seen in Figure 4.17. This was done around

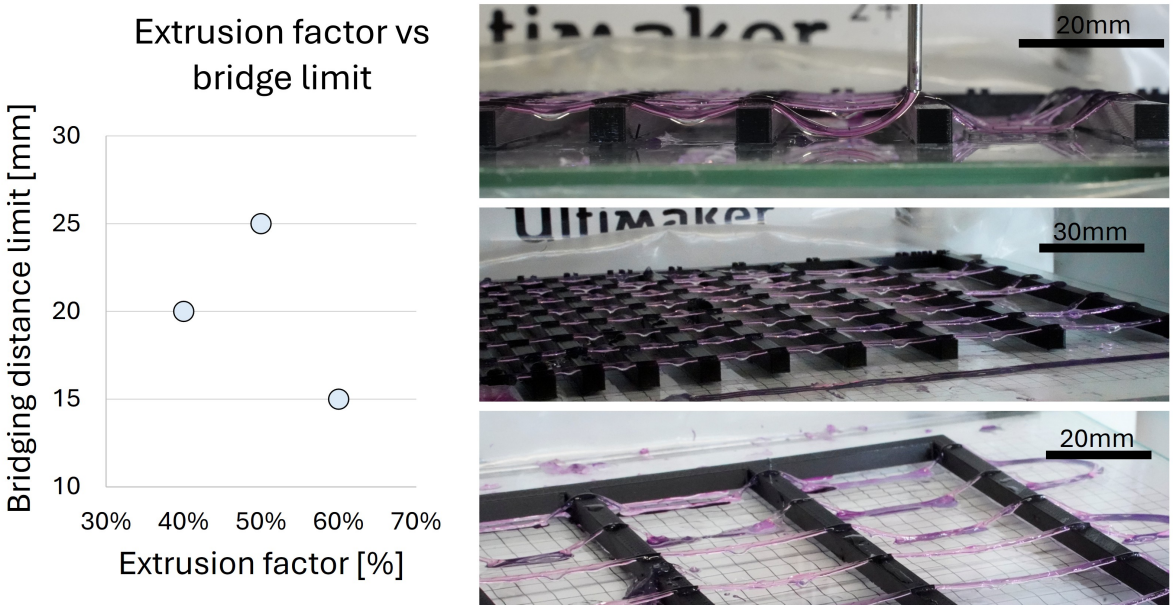

Figure 4.17: Bridging limit graph (left), bridging at EF60 (top right), bridging at EF50(middle right), bridging at EF40 (bottom right)

the stable vasculature EF of EF40, EF50, EF60. In this test a bridge was considered failed if:

1. The bridge is not vascular
2. The bridge is touching the bed

This means that collapsed, non-vascular or prints that touch the bed in any amount are omitted. For example, in Figure 4.17 EF60 print the last row is still vascular but touches the bed, while in the EF40 in the second gap, the second line has ruptured. Further, in both comb sections a total of 7 bridges could have been established - corresponding to a 100% success rate. Thus, the results of the test can be seen in Figure 4.17, Table 4.3 and Table A.2 for the EF bridge limit graph, bridging distances table for the comb up to 30 and the table for distances up to 40.

To begin with, Table 4.3 shows that for all 3 EF settings, bridging of up to 15mm is successful. Past this point the 60% profile endures a severe drop-off with the 40% and 50% vasculatures partially completing the remaining of the 30mm comb.

	Bridging Distance [mm]												
EF	**1**	**2**	**3**	**4**	**5**	**6**	**7.5**	**10**	**12.5**	**15**	**20**	**25**	**30**
40%	7	7	7	7	7	7	7	7	7	7	7	6	5
40%	7	7	7	7	7	7	7	7	7	7	7	5	5
50%	7	7	7	7	7	7	7	7	7	7	7	7	4
60%	7	7	7	7	7	7	7	7	7	7	5	0	0
Numbers in color represent the number of successful bridges out of 7													

Table 4.3: Table of number of successful bridges formed, 30mm comb

First, considering the EF60. The 60% profile has been observed to give very consistent channel formation results. This is true when printing on the bed and was used for much of the previous tests. This setting is on verge of overextrusion Figure 4.17, by this it is meant than the compounding extrusion error after a longer print may become apparent. Having this in mind, it becomes apparent why the performance of this profile drops so suddenly - there is more material being deposited and the print line droops in to the gap. Qualitatively, it can be observed from Figure 4.17 that a successful bridge is constrained by the time it takes for the vasculature to sag into contact with the bed. This time could be

reduced if the gap were cleared either at a higher F speed, higher Z offset or with more tension on the vasculature shell. Therefore, success rate can be attributed to 3 main factors:

1. Z offset height
2. Extrusion factor tension effect
3. Vasculature formation consistency

Of these effects an extrusion multiplier decrease seems to increase the experienced tension by the vasculature. Underextrusion could be quantified as an insufficient amount of material deposited per distance unit traveled. Thus, underextrusion creates vasculatures that slower that the movement of the print head. This prevents the sagging of the extrusion and thus allows for longer and longer gaps to be bridged. This is evident with the lower percentage profiles covering gaps up to 40mm, seen in Table A.2! This would be an astounding result even for a conventional FDM printer. However, there is a trade-off. Unlike the 60% profile the 40 percent is under-extruded and is prone to premature vasculature failure (similar to EF25 in Figure 4.9 caused by piercing), lack of formation. This means that with decreasing extrusion levels there is an increase of bridging distance at the cost of reliability.

Lastly, the graph in Figure 4.17 summarizes the results concisely. Here, the bridge limit is considered the farthest 100% success rate gap covered. EF50 performs the best merging the best qualities of both EF60 and EF40. The vasculatures at EF50 are stable forming, yet the tension effect is very pronounced as if at EF40. Therefore, indubitably this setting shall be selected as the nominal going forward.

4.5.1. 3D Demonstrators

Next, the final piece of the puzzle - 3D printing demonstrators. The printing of fully perfusable 3D structures is the last hurdle in conclusively validating the design of the printer. For this a cylinder and a gridlet lattice were printed.

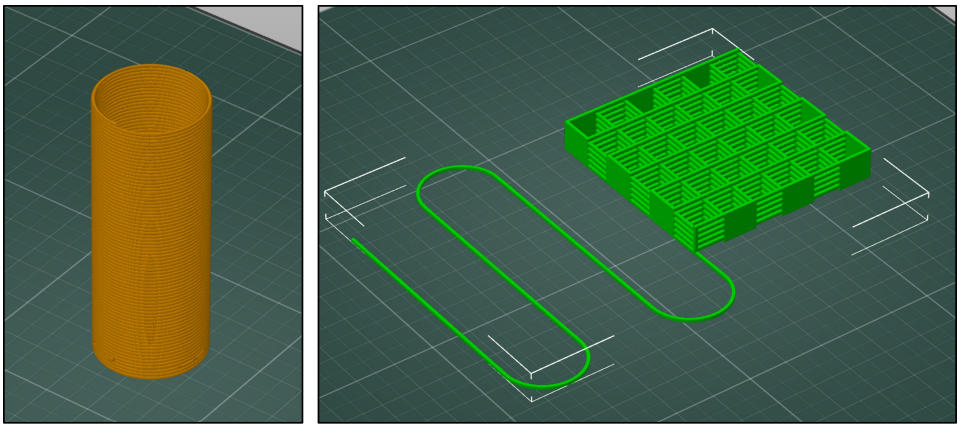

Figure 4.18: Gridlet and Cylinder 3D models

First, a tall cylinder was printed. This cylinder from Figure 4.18 is printed in vase mode showing off the variety of slicing approaches possible. Here, the goal was to push the vertical limits of the USM. Notably, this print is one wall thick and 6cm high. To emphasize, most FDM printers would struggle with printing single wall thickness tall slender structures, thus this is a difficult task considering how slippery the filament extruded is. Nevertheless, the resulting cylinder in Figure 4.19 was a success.

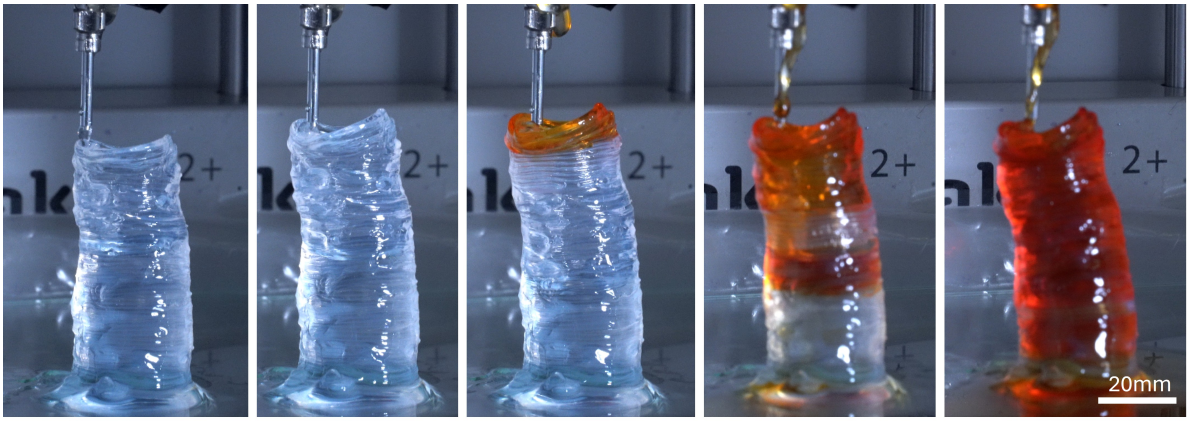

Figure 4.19: Cylinder perfusion in stages

Next, the gridlet is a overlapping lattice structure, seen in Figure 4.18. It is 10 layers high at a layer height of 0.8mm. The resulting print can be seen in Figure 4.20 (top). Here the stages of perfusion can be seen - a colourful transformation from a transparent gel to an orange, fully perfused lattice. In Figure 4.20 (bottom) it can be observed that the hollow channels that are stacked, and fused through alginate crosslinking. This constitutes a success. One particular point of interest is the ability to expand and contract the cylinder by applying additional pressure or imposing a vacuum. If designed accordingly, such structures could be used as hydraulically or pneumatically actuated compliant bio-mechanisms. Likewise, the gridlet exhibited volumetric expansion visible when comparing the not perfused section with the actively perfused (first and last in Figure 4.20).

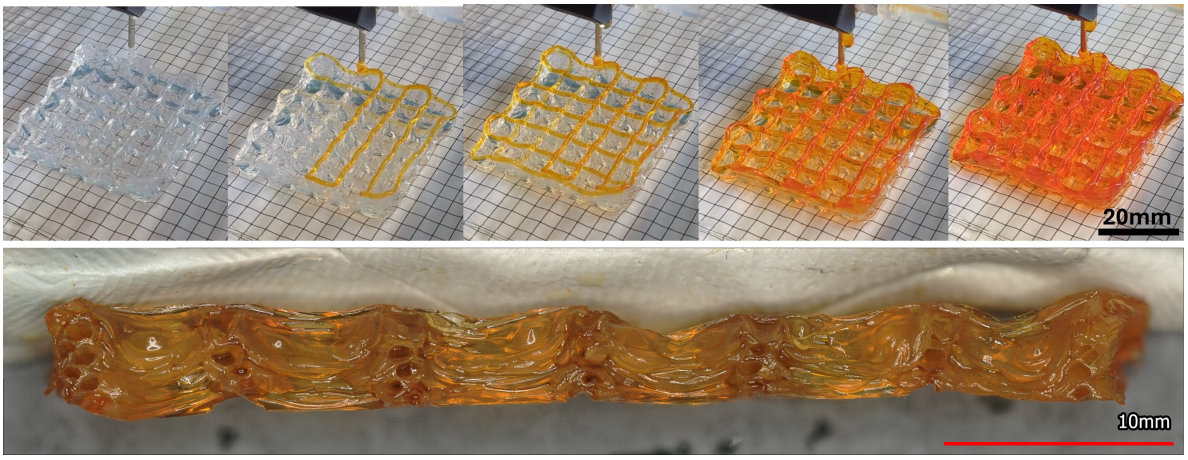

Figure 4.20: Perfusion of the gridlet (top), cross-section of gridlet (bottom)

Looking back through the whole testing and validation process the requirements can be re-evaluated once again for the final time. Similarly as in chapter 3, here in Table 4.4 the requirements that have been met are marked in dark blue, in this case it is all of them. MYCO-PRNT-01 was validated through the extrusion calibration tests in section 4.3. In the same section, MYCO-PRNT-02 was shown to be compliant by demonstrating that the inner diameter of the lumen can be controlled by changing nozzle sizes. Further, requirements MYCO-PRNT-04 and MYCO-PRNT-05 have been met in section 4.4. Controlled anlge features in the outer measurements were shown to be under 10°and radii were compliant to the 20% requirement after the feature. Last, MYCO-PRNT-06 was confirmed in section 4.5 by printing a cylinder that is larger than 4cm in height that was perfused successfully. In, summary the findings of this chapter show that the objectives of the thesis have been met, and validate the printer

by fulfilling the complete set of requiremetns.

#	REQ ID	Validation Method	Verification Comments	Description
1	MYCO-PRNT-01	Test	Verified through test	The 3D printer shall produce prints capable of perfusion of 20 ml
2	MYCO-CAD-01	Review of Design	SuperSlicer can slice files In particular format.	The 3D printer software suite shall allow for slicing .stl and .3mf files
3	MYCO-PRNT-02	Test	Demonstrated the possibility to vary vasculature sizing	The 3D printer shall be able to print vasculatures of 3 different ID
4	MYCO-SAFE	Review of Design, Inspection	Waterproofing and emergency stops are present	The 3D printer shall have measures to prevent user error damage to the printer
5	MYCO-DESIGN-01	Review of Design, Inspection	Nozzle is modular, accommodates different diameter needles	The 3D printer shall have a modular nozzle
6	MYCO-INK	Review of Design	Printer has been developed using these inks	The 3D printer shall support printing in alginate and calcium chlorate
7	MYCO-PRNT-04	Test	Demonstrated through test	The 3D printer shall print perfusable planar angles with an error after the feature, no greater than 10 deg
8	MYCO-PRNT-05	Test	Demonstrated through test	The 3D printer shall print perfusable planar radii with an error after the feature , no greater than 20%
9	MYCO-PRNT-06	Test	Demonstrated through test	The 3D printer shall be able to print a perfusable structures of 4cm in height
10	MYCO-DESIGN-02	Review of Design, Inspection	Final iteration does not leak	The modular nozzle shall not leak
11	MYCO-DESIGN-03	Review of Design, Inspection	Concentricity of final nozzle achieved	The distance between the inner and outer needle walls shall be larger than 1 wall thickness of the inner needle

Table 4.4: Requirement verification table. Dark blue represent requirements that have been met.

5

Conclusions

To begin with, a key outcome of the thesis is a validated functioning 3D coaxial bioprinter. The results of this validation campaign show, in summary that the printer can vary the size of the vasculature, print complex shapes and 3D structures while perfusable.

The first series of results quantify the ability to print vasculatures of varying diameters and show it is possible to introduce features by varying parameters. It was found that by changing the extrusion factor EF, it is possible to induce meandering, stable or closed channel features corresponding to over, stable and under extrusion, respectively. Moreso, the linear behaviour of the dispensing of ink through gcode commands and EF was validated, enabling the precise estimation of ink dispensed. Further, it was confirmed that increasing nozzle size increases the inner diameter of the channel. Additionally, from comparing optical and volumetric measurements it was concluded that the inner channel cross section is likely elliptical due to gravity effects.

Next, the planar experiment series covered the accuracy of printing sharp and round planar features. Here, it was found that sharp angles are some what opened up by the internal stiffness of the vasculature. The effect was found to be greatest at the feature, with being attenuated as the distance from the feature increases. From the U test it was found that for round, radius constrained features - at the feature the radius of the feature becomes tighter. This is thought to be the vasculature being dragged inwards by the print head while closing the radius. For sections that are straight lines close to each other the excess alginate pushes the channels slightly apart. This effect is subdued by at sufficient gaps. Furthermore, once printed in a complex compound shape including various sharp and radial features, these effects can be seen as well, however this is of no concern since the errors occur consistently and functional 3D prints can be achieved.

Lastly, the bridging test demonstrated a capability to bridge gaps of up to 40+mm. The bridging was found to be an effect of sagging time, which could be reduced by increasing Z offset, F speed or reducing the EF. Reducing the EF increases the tension experienced by the vasculature. A trade-off was found that low EF although good in bridging is prone to vasculature formation failures, while high EF gives stable formation with weak bridging. Thus, based on the results the EF50 profile was selected as the nominal profile. With this two demonstrators, a cylinder and gridlet were successfully printed and perfused using the technique developed during the thesis.

6

Recommendations

6.1. Challenges & Recommendations

Many challenges come up when attempting printing precise 3D vascular structures. One of such challenges is the clogging first mentioned in chapter 2. In this thesis the solution was to introduce a modular nozzle that can be cleaned, however this does not solve the initial issue of clogging itself. For this a solution based on the EDTA approach discussed in subsection 3.3.1, but instead of ETDA another solvent could be investigated that is more aggressive and effective. This of course could be also solved by changing the ink formulation altogether, swapping to a UV activated pluronic or such.

Next, the quality of the prints and consistency could be somewhat improved by introducing a triaxial setup. By flowing calcium chloride on the outside as well as the inside, the cross-linking on the outside should produce a stiffer, and more circular vasculature as it were to be printed in a bath. A triaxial setup could be created by simply screwing up the existing modular nozzles bodies with an additional even smaller inner needle. For this a 10G-16G-24G pairing could be used. Moreover, an additional stepper with a syringe should then be added. This would then also enable the research or triaxial biomaterials, in case other inks would be explored.

Further, a large challenge is the continuous perfusion and sterile incubation of prints. This means that any print with life inoculated are separated from the nozzle and incubated. The handling off off the bed may affect the geometry of the print and therefore the subsequent growth. For this to be solved, the prints should be printed on to a Petri dish, and thus an excluded volume should be programmed either into the printer or the slicing of the file, with some standard dish sizes. To add, to solve the perfusion after incubation and throughout, a transfer jig should be made to hold the nozzle in the same position when first perfused, so that the whole dish could be moved at once. This would essentially make a stable luer attach point for easy perfusion and since the nozzles are abundant and easy to make, many specimens could be incubated and perfused at a time. Otherwise, this can be solved by pursuing an alginate block based approach mentioned in subsection 4.1.4 and developing some sort of manual perfusion technique/interface.

Last, the printing process could go through additional tuning. For instance, the errors seen in section 4.4 could be mitigated by adjusting the slicer software to account for this. To do this testing can be done to quantify, for instance, the additional EF needed to reduce turn radius errors, or perhaps, angle compensation processing for sharp corners, gradually compensating the error throughout the path.

6.2. Future Outlook

The future of bioprinting of vasculature is one full of sci-fi innovation and everyday application in medicine, electronics and more. For one fungi is known to emit electrical voltages under UV exposure or other stimuli. Vascular structures could embed and feed fungi maintaining an alive state in structures to measure the experienced stress. Perhaps in the future a fungi building could inform you that your house is about to collapse and needs reinforcement, allowing us to build smart bio-enabled

structures. Another, feature enabled by vasculature bioprinting could be printing of bio structures in situ. The design produced during this thesis is not constrained to the printer space by a bath of sorts, this allows one to utilise the print head on a robotic arm or other on the go device. A future where fire victims can get a tailored perfusable gauze minutes after a fire occurs could perhaps save lives and prevent scarring. Finally, vascular printers could remodel the framework under which research in bio-samples is made, by offering a perfusable stage between wet grown and solid state grown cultures.

References

[1] Eman Mirdamadi et al. “FRESH 3D Bioprinting a Full-Size Model of the Human Heart”. In: *ACS Biomaterials Science & Engineering* 6.11 (Nov. 2020). Publisher: American Chemical Society, pp. 6453–6459. DOI: 10.1021/acsbiomaterials.0c01133. URL: https://doi.org/10.1021/acsbiomaterials.0c01133 (visited on 11/11/2025).

[2] Qing Gao et al. “Coaxial nozzle-assisted 3D bioprinting with built-in microchannels for nutrients delivery”. In: *Biomaterials* 61 (Aug. 2015), pp. 203–215. ISSN: 0142-9612. DOI: 10.1016/j.biomaterials.2015.05.031. URL: https://www.sciencedirect.com/science/article/pii/S0142961215004810 (visited on 11/12/2025).

[3] Abraham Samuel Finny. “3D bioprinting in bioremediation: a comprehensive review of principles, applications, and future directions”. en. In: *PeerJ* 12 (Feb. 2024). Publisher: PeerJ Inc., e16897. ISSN: 2167-8359. DOI: 10.7717/peerj.16897. URL: https://peerj.com/articles/16897 (visited on 07/07/2025).

[4] Benjamin A. E. Lehner, Dominik T. Schmieden, and Anne S. Meyer. “A Straightforward Approach for 3D Bacterial Printing”. In: *ACS Synthetic Biology* 6.7 (July 2017). Publisher: American Chemical Society, pp. 1124–1130. DOI: 10.1021/acssynbio.6b00395. URL: https://doi.org/10.1021/acssynbio.6b00395 (visited on 07/07/2025).

[5] Sean V. Murphy and Anthony Atala. “3D bioprinting of tissues and organs”. en. In: *Nature Biotechnology* 32.8 (Aug. 2014). Publisher: Nature Publishing Group, pp. 773–785. ISSN: 1546-1696. DOI: 10.1038/nbt.2958. URL: https://www.nature.com/articles/nbt.2958 (visited on 07/07/2025).

[6] Tarun Shyam Mohan et al. “3D coaxial bioprinting: process mechanisms, bioinks and applications”. en. In: *Progress in Biomedical Engineering* 4.2 (Apr. 2022). Publisher: IOP Publishing, p. 022003. ISSN: 2516-1091. DOI: 10.1088/2516-1091/ac631c. URL: https://dx.doi.org/10.1088/2516-1091/ac631c (visited on 07/04/2025).

[7] Ke Zheng et al. “Recent progress of 3D printed vascularized tissues and organs”. In: *Smart Materials in Medicine* 5.2 (June 2024), pp. 183–195. ISSN: 2590-1834. DOI: 10.1016/j.smaim.2024.01.001. URL: https://www.sciencedirect.com/science/article/pii/S2590183424000127 (visited on 07/07/2025).

[8] Tao Jiang et al. “Extrusion bioprinting of soft materials: An emerging technique for biological model fabrication”. In: *Applied Physics Reviews* 6.1 (Mar. 2019), p. 011310. ISSN: 1931-9401. DOI: 10.1063/1.5059393. URL: https://doi.org/10.1063/1.5059393 (visited on 07/08/2025).

[9] Falguni Pati et al. “Chapter 7 - Extrusion Bioprinting”. In: *Essentials of 3D Biofabrication and Translation*. Ed. by Anthony Atala and James J. Yoo. Boston: Academic Press, Jan. 2015, pp. 123–152. ISBN: 978-0-12-800972-7. DOI: 10.1016/B978-0-12-800972-7.00007-4. URL: https://www.sciencedirect.com/science/article/pii/B9780128009727000074 (visited on 07/08/2025).

[10] Thomas J. Hinton et al. “Three-dimensional printing of complex biological structures by freeform reversible embedding of suspended hydrogels”. In: *Science Advances* 1.9 (Oct. 2015). Publisher: American Association for the Advancement of Science, e1500758. DOI: 10.1126/sciadv.1500758. URL: https://www.science.org/doi/10.1126/sciadv.1500758 (visited on 07/08/2025).

[11] Kuen Yong Lee and David J. Mooney. “Alginate: properties and biomedical applications”. eng. In: *Progress in Polymer Science* 37.1 (Jan. 2012), pp. 106–126. ISSN: 0079-6700. DOI: 10.1016/j.progpolymsci.2011.06.003.

[12] Mohammad Shafiur Rahman. *Handbook of food preservation*. eng. second edition. Food science and technology 167. Boca Raton (Fla.): CRC press, 2007. ISBN: 978-1-57444-606-7.

[13] Farzaneh Dolati et al. “In vitro evaluation of carbon-nanotube-reinforced bioprintable vascular conduits”. en. In: *Nanotechnology* 25.14 (Mar. 2014). Publisher: IOP Publishing, p. 145101. ISSN: 0957-4484. DOI: 10.1088/0957-4484/25/14/145101. URL: https://doi.org/10.1088/0957-4484/25/14/145101 (visited on 11/12/2025).

[14] Guoliang Ying et al. “Three-dimensional bioprinting of gelatin methacryloyl (GelMA)”. en. In: *Bio-Design and Manufacturing* 1.4 (Dec. 2018), pp. 215–224. ISSN: 2522-8552. DOI: 10.1007/s42242-018-0028-8. URL: https://doi.org/10.1007/s42242-018-0028-8 (visited on 11/12/2025).

[15] Jaroslaw M. Wasikiewicz et al. “Degradation of chitosan and sodium alginate by gamma radiation, sonochemical and ultraviolet methods”. In: *Radiation Physics and Chemistry* 73.5 (Aug. 2005), pp. 287–295. ISSN: 0969-806X. DOI: 10.1016/j.radphyschem.2004.09.021. URL: https://www.sciencedirect.com/science/article/pii/S0969806X04005626 (visited on 10/25/2025).

[16] Hao Lu et al. “Natural Antimicrobial Nano Composite Fibres Manufactured from a Combination of Alginate and Oregano Essential Oil”. en. In: *Nanomaterials* 11.8 (Aug. 2021), p. 2062. ISSN: 2079-4991. DOI: 10.3390/nano11082062. URL: https://www.mdpi.com/2079-4991/11/8/2062 (visited on 11/09/2025).

A

Appendix

Table A.1: Table of Bio-Inks [6]

#	Shell bioink or crosslinker	Core bioink or crosslinker	Cell type used	Ref.
1	GelMA	Peptide-functionalized, succinylated chitosan (C)/dextran aldehyde (D)	Shell - hBMSCs	
2	GelMA	Gelatin	Shell: HUVECs, MC3T3-E1 or MDA-MB-231; Core: ECs	
3	Alg/SF	Pluronic F127 and calcium ions	C3A liver cancer cells	
4	Gelatin-PEG-tyramine (GPT) prepolymer	Gelatin	Shell: HDFs; Core: HUVECs	
5	Sodium alginate	Gelatin and alginate	Core: NE-4C	
6	Gelatin-GelMA	PVA	Shell: HUVECs	
7	ALG-CMC-NFC	Calcium chloride	HUVECs	
8	Calcium chloride	ALG, GelMA and β-tricalcium phosphate (TCP)	Core: BM-hMSCs	
9	Sodium alginate	GelMA and calcium chloride	Core: GFP-HUVECs	
10	GelMA	Alginate	Shell: EPC; Core: islets cells	
11	Calcium alginate	GelMA	Core: HUVECs	
12	Alginate	Cell suspension	Shell: GSC23; Core: U118	
13	GelMA, alginate and eight-arm poly(ethylene glycol) acrylate with a tripentaerythritol core	Calcium chloride	Shell: Various cell types	
14	HA-GelMA and photoinitiator (VA-086)	HA-GelMa	Core: MSCs	
15	Alginate	GelMA and calcium chloride	Core: HUVECs	
16	Alginate/gelatin	Fibrinogen	Core: RFP-GSCs and GFP-MSCs	
17	Calcium chloride	Alginate, GelMA, chondroitin sulfate amino ethyl methacrylate (CS-AEMA) and HAMA (optional)	Core: BM-MSCs	
18	Calcium chloride	GelMA, alginate and a photoinitiator (LAP)	Core: HUVECs	
19	algMC + matrigel	algMC; algMC + fibrin; or algMC + plasma	Shell: HepG2; Core: NIH 3T3	

	Bridging Distance [mm]		
EF	**30**	**35**	**35**
40%	5	5	4

Table A.2: Larger comb (up to 40mm) test results

B

Supplementary figures

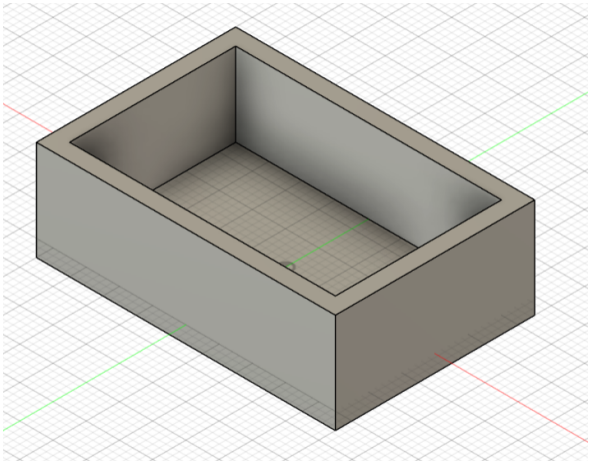

Figure B.2: CAD model of Alginate block mould

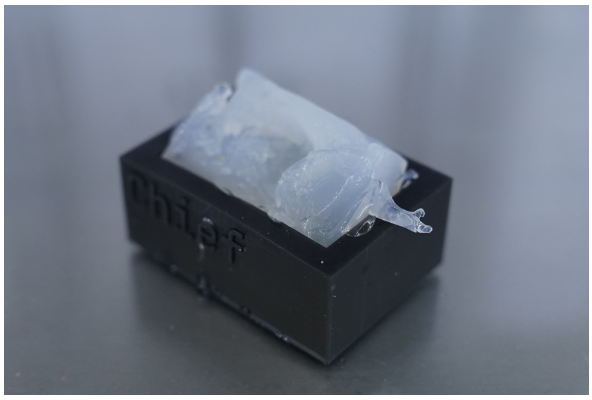

Figure B.3: Cast Alginate Block

Notably, there are 3 main menus of importance in the environment. The print settings Figure B.5a, the filament settings Figure B.5b and the printer settings Figure B.5c.

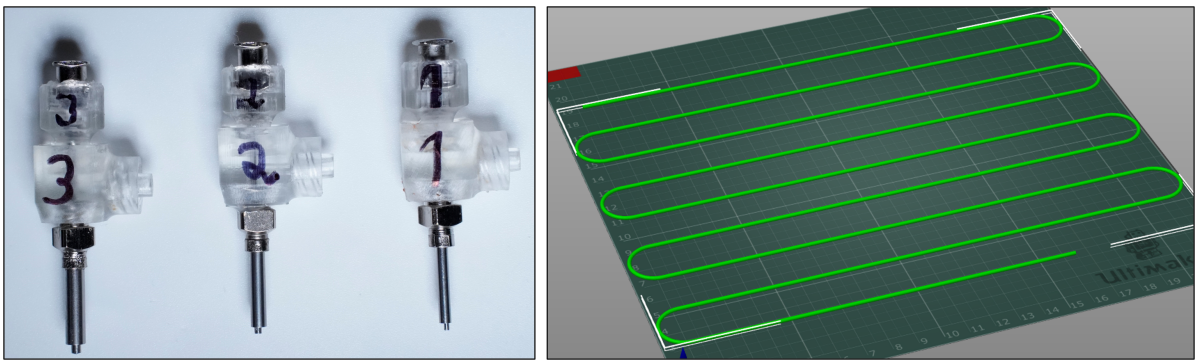

Figure B.1: 3 nozzle combinations used in nozzle tests (left), ”Bedzag” print 3D model (right)

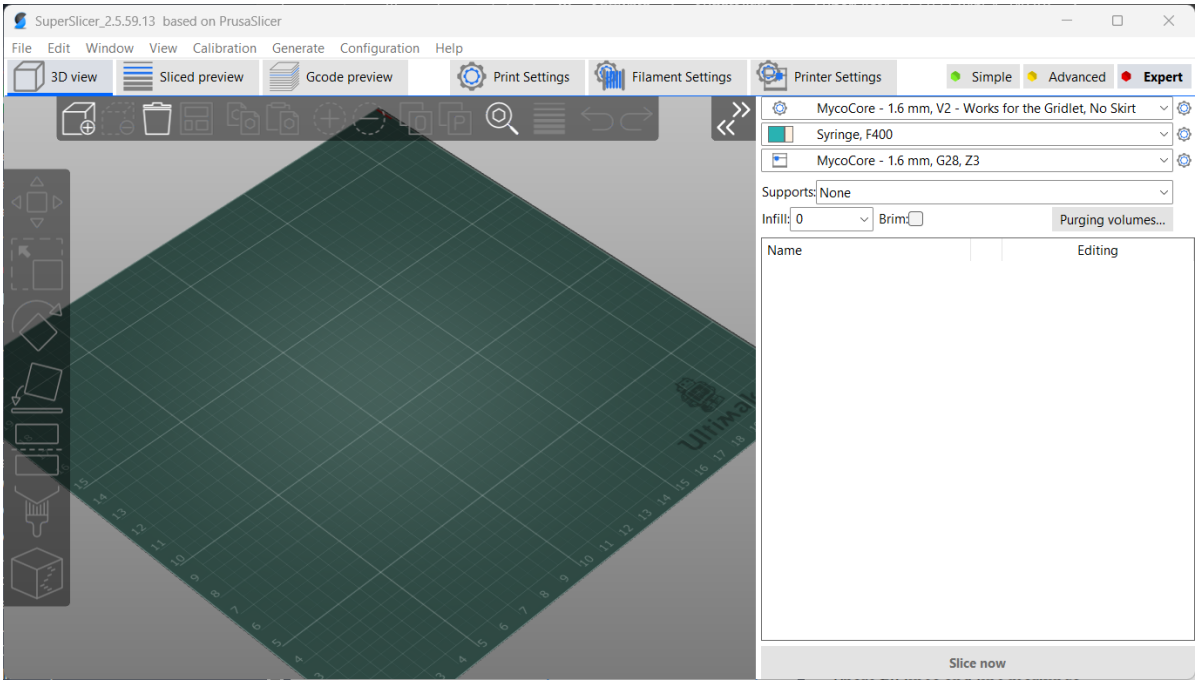

Figure B.4: Superslicer Environment

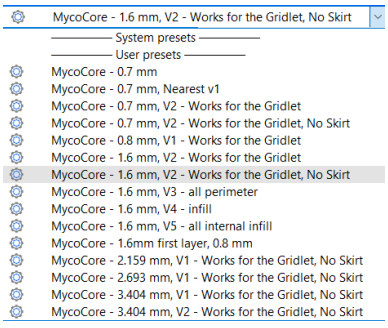

(a) Print Settings Menu

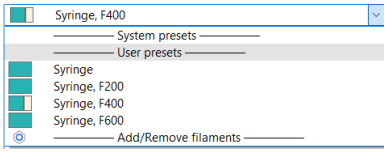

(b) Filament Settings Menu

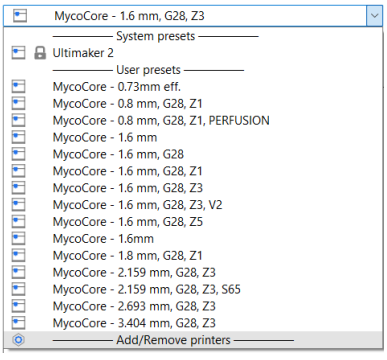

(c) Printer Settings Menu

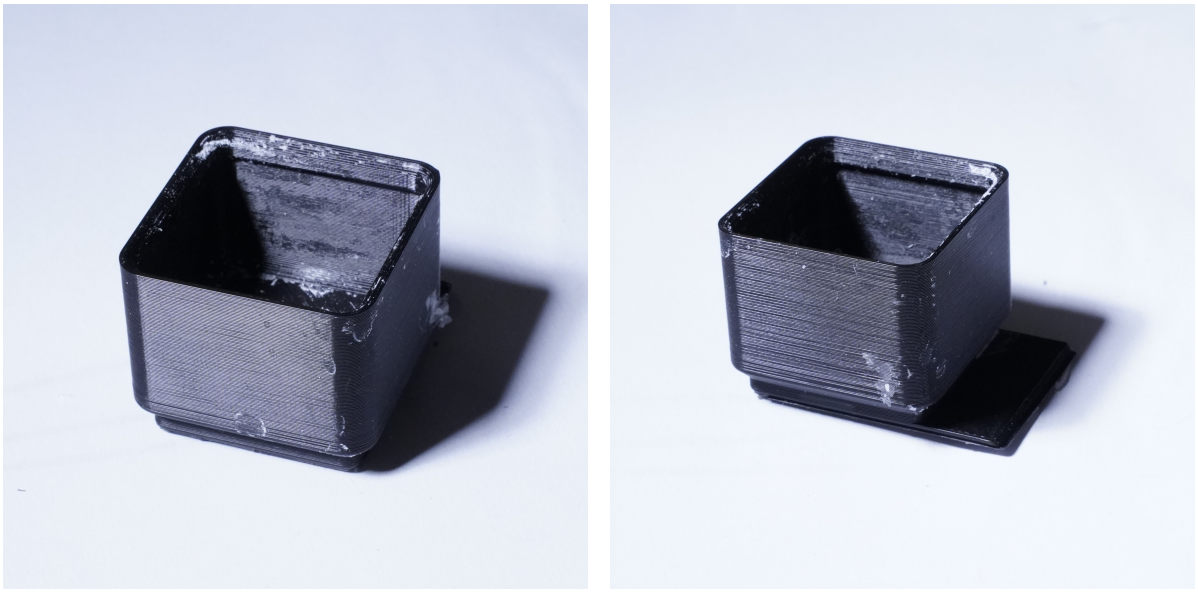

Figure B.6: EDTA bath

Figure B.7: Waterproofing wrapped enclosure

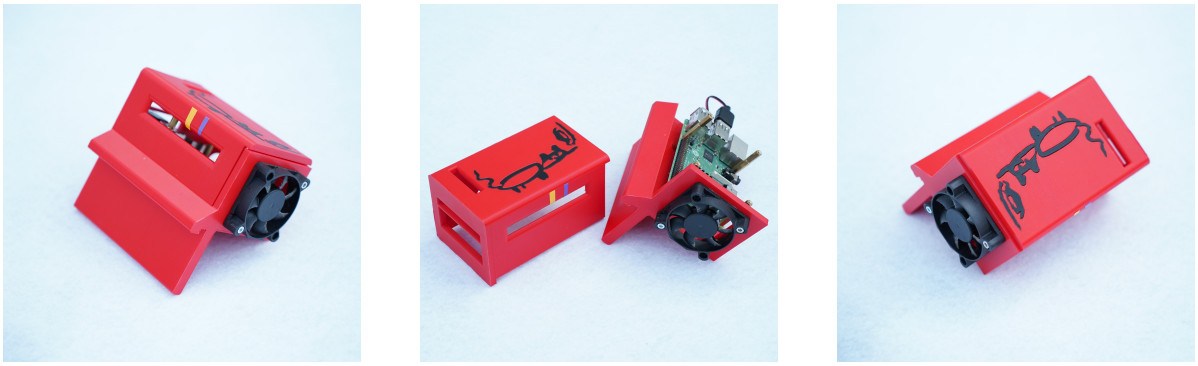

Figure B.8: Electronics Case

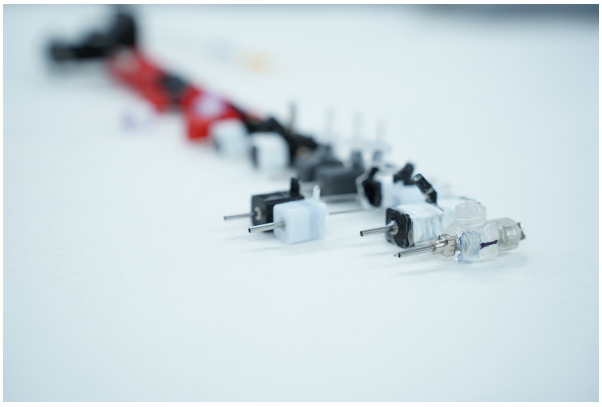

Figure B.9: Luer lock nozzle spotlight